

Statistics of the largest eigenvalues and singular values of low-rank random matrices with non-negative entries

Mark J. Crumpton,* Yan V. Fyodorov, and Pierpaolo Vivo

Department of Mathematics, King's College London, London WC2R 2LS, United Kingdom

(Dated: August 22, 2022)

We compute analytically the distribution and moments of the largest eigenvalues/singular values and resolvent statistics for random matrices with (i) non-negative entries, (ii) small rank, and (iii) prescribed sums of rows/columns. Applications are discussed in the context of Mean First Passage Time of random walkers on networks, and the calculation of network “influence” metrics. The analytical results are corroborated by numerical simulations.

I. INTRODUCTION

Matrices with non-negative entries (NNEMs) occur frequently in many applications. First of all, they prominently feature in the context of Markov chains on complex networks. Markov chains (e.g. random walks) are stochastic processes in memory-less systems, such that the next state of the system – typically, the next node visited by the walker – depends only on the current state (node occupied) [1, 2] and not on the full history of how the walker got there in the first place. In such processes, the adjacency matrix A_{ij} of a network has $\{0, 1\}$ entries depending on whether a link exists between node i and node j . The adjacency matrix is then normalised according to the out-strength k_i of each node to give a normalised transition-probability matrix $\pi_{ij} = A_{ij}/k_i$ [3], representing the (in this simple setting, unbiased) probability that the walker reaches node j starting from node i . Row and column stochastic matrices, whose (i, j) entry is the probability that a Markov process jumps from site i to site j , are very important in determining the long-time equilibrium distribution of probabilistic processes [4]. Analytical and numerical results are available for row (column) stochastic matrices, where the entries in each row (column) sum to one, and doubly stochastic matrices, where the entries in all rows and columns sum to one [5–8]. These results include e.g. conditions for similarity between row and doubly stochastic matrices, limits of convergence of a non-negative matrix to a doubly stochastic matrix by alternate scaling of rows and columns, mixing time of Markov chains and methods to generate doubly stochastic matrices.

Another prominent application of NNEMs comes in the field of economics, namely the input-output matrices developed by Leontief [9]. These matrices are used to assess how much of the output of one economic sector is needed as an input to another sector for a complex economy to work, providing quantitative indicators (such as *upstreamness* and *downstreamness* [10–12]) of relationships and inter-dependence between different sectors [13]. The study of NNEMs arises naturally in a wide range of economic areas, due to the non-negative nature of many economic quantities, such as exchange rates, expenses, and productivity measures [14–17]. Additionally, recent research into the so-called Leontief inverse, which relates total output and demand of economic sectors, has led to the realisation that these matrices have universal features that can be applied to a wide range of economies [18].

Further applications of NNEMs can be found in Game Theory, for example the payoff matrix, used to determine optimal in-game strategies [19, 20]. Moreover, NNEMs arise naturally in the study of singular values and singular value decomposition, where the diagonal matrix of singular values is non-negative by definition [21]. Many more interesting problems that rely on the study of NNEMs are outlined in [22]. Among a few examples worth mentioning are the pricing of houses, and optimal scheduling of tasks in work environments with the aim to create fair divisions of quantities to respect the needs of individuals.

One important feature for the study of NNEMs is the Perron-Frobenius theorem. This was first developed in the early 20th century by Oskar Perron for positive matrices [23, 24], and was then generalised to irreducible matrices by Georg Frobenius in 1912 [25–27]. It states that for such matrices an NNEM will have one real eigenvalue λ_r , such that all the other (in general complex) eigenvalues have magnitudes $\leq |\lambda_r|$. Additionally, it states that the eigenvector corresponding to λ_r will have strictly non-negative elements. All other eigenvectors have at least one negative element.

To study generic and potentially universal spectral features shared by NNEMs of diverse nature it makes sense to consider ensembles of NNEMs with random entries. In such a setting, a natural problem to study is the distribution of the Perron-Frobenius (largest) eigenvalue (or singular value), whose magnitude and distance from the second-largest eigenvalue are known to govern various interesting phenomena, including many features of dynamical processes on

* mark.j.crumpton@kcl.ac.uk

networks [28]. The existence of a large spectral gap between the two largest eigenvalues of a matrix manifests itself, e.g., when one considers a Gaussian perturbation of a rank-1 matrix. Any matrix with entries drawn as iid mean zero Gaussian random variables of variance σ^2/N will have its eigenvalues located within a disk of radius σ in the complex plane. This phenomenon is known as the Girko-Ginibre circular law [29, 30]. Adding a matrix of this form to a rank-1 matrix does not affect this bulk circle of eigenvalues but can lead to the presence of an outlier, if the potential outlier eigenvalue has a value greater than some threshold depending on σ . Therefore, if the Gaussian perturbation is too large, the outlier is not seen as separated from the bulk. It is precisely the interplay between this bulk of eigenvalues and the outlier that has attracted a wealth of attention in recent research due to its relevance in data processing [31–33].

The study of matrices generated as the sum of a Gaussian and a rank-1 matrix can be extended further when one adds in the positivity constraint for the entries of the rank-1 matrix. Note that any Gaussian matrix with nonvanishing variance results in a non-vanishing probability to get negative entries in the matrix given by the sum of the Gaussian and the rank-1 matrix. This has interesting implications in the context of Markov chains, where a phase transition controlled by a temperature-like variable has been shown to exist [34]. Markov processes are described by stochastic matrices whose properties are well-known in the limit of large matrix size. The temperature-like variable which controls the variance of the elements in the stochastic transition matrix is defined in such a way that a ‘high-temperature’ corresponds to a matrix with a small spread in its elements and vice versa for ‘low-temperature’ matrices. Such a variable describes a certain parameter regime below which the standard random matrix theory results for large stochastic matrices do not hold. The onset of this regime is given by a critical temperature, defined by the condition of the radius of the circular bulk being equal to unity, implying that the spectral gap goes to zero. In particular, for matrices with a temperature below the critical temperature the standard circular law for the eigenvalues of a stochastic matrix [33] does not hold. Instead, one finds a situation where the eigenvalues remain in a circular bulk of unit radius but ‘spokes’ begin to emerge along the roots of unity [34]. Additionally, in the context of the Mean First Passage Time (MFPT) that a random walker takes to reach a target node on a complex network, a large gap between the Perron-Frobenius eigenvalue of the transition matrix and the bulk of all the other eigenvalues guarantees that a fast, approximate formula works without the need for heavy matrix inversions [35].

While the study of Extreme Value Statistics is probably one of the most developed corners of Random Matrix Theory since the discovery of the celebrated Tracy-Widom distribution [36], the research on random NNEMs instead has so far mostly focused on permanents, averages, and products [37–41], whereas spectral features have been addressed mainly via bounds, iterations, and inequalities [42–44]. Partly this bias is probably due to the fact that the spectral properties of random NNEMs turn out to be quite difficult to characterise exactly. Indeed, one may notice that the non-negativity constraint on the entries (i) is bound to break the rotational invariance of any model - thus ruling out the most powerful analytical tools available (orthogonal polynomials, determinantal processes etc.), and (ii) cuts the domain of integration of variables and forces non-Gaussian multiple integrals into the standard cavity or replica treatments [45] – which quickly leads to insurmountable computational challenges.

From this angle, one way to make progress in the analytical study of spectral properties of NNEMs is to consider a simplified scenario where the matrix (i) is low-rank, and (ii) has a prescribed set of row/column sums. Low-rank matrix approximations in the context of NNEMs are known to be very useful [46], as in this case there are only a handful of non-zero eigenvalues/singular values that need to be taken into consideration, which can usually be easily linked to the row/column sums. Moreover, such matrices arise naturally in several ‘matrix reconstruction’ schemes based on the Maximum Entropy method, with applications e.g. to inter-bank network reconstruction [47–49]. Approximations using low-rank matrices have also been utilised in the study of dissipative quantum transport, the N -body problem and fluid dynamics [50–52].

Furthermore, the analysis of random NNEMs can be extended to consider their resolvents, or Green functions. The resolvent is an object of high utility which can be employed to calculate spectral densities of matrices using complex analysis [53]. Moreover, the resolvent of low-rank matrices with prescribed row/column sums appears naturally in many of the problems discussed above (Leontief Input/Output coefficients, MFPT of walkers on random networks), as well as in the calculation of the “influence” of nodes in a complex network [54] or the location of outlier eigenvalues in random matrix ensembles related to networks [55].

In this work, we succeed in characterising analytically statistical features of the non-zero eigenvalues, singular values, and resolvents of random rank-1 and rank-2 NNEMs with prescribed row/column sums, along with accurate large N approximations that are computationally simpler to evaluate. All theoretical results are validated through numerical simulations. The models studied in this work are rare examples of $N \times N$ matrices where the full Extreme Value statistics and interesting spectral observables can be computed *for finite N* (and not just for large N).

In Sec. II we present a model for a general rank-1 NNEM where the sums of the elements in each row are fixed. The way in which the sum is partitioned across the rows is controlled by a vector of flat Dirichlet random variables and, in order to analyse spectral properties of this model, we perform averages over this vector. In this way for any finite matrix size N we find exact formulas for the distribution of the Perron-Frobenius eigenvalue and all integer moments

of the only non-zero eigenvalue and singular value squared. Large N approximations to the eigenvalue and singular value distributions are also discussed. Then in Sec. III we present a one-parameter family of random rank-2 NNEMs, derived as an extension of the rank-1 model, where the sum of the elements in each column are also fixed. Executing the average over all possible NNEMs in this family allowed us to derive exact formulas for the distribution of the sum and product of the non-zero eigenvalues and singular values. The distributions involving the non-zero singular values are particularly noteworthy due to the presence of discontinuities arising as a result of certain values corresponding to different numbers of solutions. In Sec. IV the entries of the resolvent vector of both the rank-1 and one-parameter family of rank-2 NNEMs are also presented. In the rank-1 case we discuss the one point marginal density of the entries in the resolvent vector both exactly and with an accurate large N approximation. The entries of the resolvent vectors of these matrix approximations are then compared to an exact value and results generated using a pre-existing low-rank matrix formulation [35]. This comparison shows that the one-parameter family of rank-2 NNEMs produces highly accurate approximations to the MFPT of a random walker on a complex network. Finally, in Sec. V we summarise our findings with some concluding remarks and provide an outlook on potential future developments of our study.

II. RANK-1 NNEMS

In a rank-1 matrix, the elements in each column are multiples of some basis vector, ensuring that column vectors are not linearly independent (i.e. the column vectors form a vector space of dimension 1). This leads to the matrix having only one non-zero eigenvalue and one non-zero singular value. For a real rank-1 matrix M this eigenvalue is given by $\text{Tr}(M)$ and the singular value is given by $\sqrt{\text{Tr}(M^T M)}$.

As a warm-up setting, we consider a generic $N \times N$ rank-1 NNEM constructed as

$$T_1 = \mathbf{z}\mathbf{a}^T = \begin{pmatrix} a_1 z_1 & a_2 z_1 & \cdots & a_N z_1 \\ a_1 z_2 & a_2 z_2 & \cdots & a_N z_2 \\ \vdots & \vdots & \ddots & \vdots \\ a_1 z_N & a_2 z_N & \cdots & a_N z_N \end{pmatrix}, \quad (1)$$

where \mathbf{z} is a column vector containing the prescribed (non-negative) row sums ($\mathbf{z} = (z_1, z_2, \dots, z_N)^T$), which we assume are all distinct, and \mathbf{a} is a column vector of random non-negative variables satisfying the only constraint that $\sum_i a_i = 1$. In what follows we call such a vector *flat Dirichlet-distributed*.

The marginal density of each a_i can be derived as

$$p_N(a_i) = \frac{\int_{\mathbb{R}_+^{N-1}} da_1 \cdots da_{i-1} da_{i+1} \cdots da_N \delta\left(\sum_{i=1}^N a_i - 1\right)}{\int_{\mathbb{R}_+^N} da_1 \cdots da_N \delta\left(\sum_{i=1}^N a_i - 1\right)} = \Theta[a_i] \Theta[1 - a_i] (N-1)(1 - a_i)^{N-2}, \quad (2)$$

where $\mathbb{R}_+ := [0, \infty)$ and $\Theta[x]$ is the Heaviside function ($\Theta[x] = 1$ for $x > 0$ and $\Theta[x] = 0$ for $x \leq 0$).

One may then ask, what is the distribution of the only non-zero (Perron-Frobenius) eigenvalue and the only non-zero singular value due to the chosen randomness in the a_i 's? In the next subsections we provide the answer to this question. Later on, in Sec. IV, we will also consider the resolvent statistics of this class of matrices in the context of mean first passage times and network influence.

A. Non-zero eigenvalue (Perron-Frobenius)

The only non-zero eigenvalue of T_1 has the simple form

$$\lambda = \sum_{i=1}^N a_i z_i, \quad (3)$$

leading to the following expression for its probability density function (pdf)

$$P_{\mathbf{z},N}(\lambda) = C_N \int_0^\infty da_1 \int_0^\infty da_2 \cdots \int_0^\infty da_N \delta\left(\sum_{i=1}^N a_i - 1\right) \delta\left(\lambda - \sum_{i=1}^N a_i z_i\right), \quad (4)$$

where $C_N = (N - 1)!$ is the normalisation constant.

To evaluate the above we first consider the auxiliary function

$$P_{\mathbf{z},N}(\lambda, t) = C_N \int_0^\infty da_1 \int_0^\infty da_2 \cdots \int_0^\infty da_N \delta\left(\sum_{i=1}^N a_i - t\right) \delta\left(\lambda - \sum_{i=1}^N a_i z_i\right) \quad (5)$$

and its double Laplace transform w.r.t. λ and t

$$\begin{aligned} \tilde{P}_{\mathbf{z},N}(\mu, s) &= \int_0^\infty d\lambda e^{-\lambda\mu} \int_0^\infty dt e^{-st} P_{\mathbf{z},N}(\lambda, t) = C_N \int_0^\infty da_1 \int_0^\infty da_2 \cdots \int_0^\infty da_N \exp\left[-s \sum_{i=1}^N a_i - \mu \sum_{i=1}^N a_i z_i\right] \\ &= C_N \prod_i \int_0^\infty da_i e^{-sa_i - \mu a_i z_i} = C_N \prod_i \frac{1}{s + \mu z_i}. \end{aligned} \quad (6)$$

This can be easily inverted yielding

$$P_{\mathbf{z},N}(\lambda, t) = (N - 1) \sum_{k=1}^N \frac{z_k^{N-2}}{\prod_{l \neq k} (z_k - z_l)} \left(t - \frac{\lambda}{z_k}\right)^{N-2} \Theta\left[t - \frac{\lambda}{z_k}\right] \quad (7)$$

and after setting $t = 1$ we arrive at

$$P_{\mathbf{z},N}(\lambda) = (N - 1) \sum_{k=1}^N \frac{1}{\prod_{l \neq k} (z_k - z_l)} (z_k - \lambda)^{N-2} \Theta[z_k - \lambda]. \quad (8)$$

The spectral range supporting the eigenvalues can be obtained by analysing the form of this pdf. Firstly, it is evident that when $\lambda \geq \max(z_1, z_2, \dots, z_N)$, the pdf goes to zero as a consequence of the vanishing Θ functions. Less trivial is to show that when $\lambda \leq \min(z_1, z_2, \dots, z_N)$ the pdf also goes to zero. For this we use that with Θ functions all yielding simultaneously the same value 1, we can apply the following identity,

$$\sum_{k=1}^N \frac{z_k^m}{\prod_{l \neq k} (z_k - z_l)} = \begin{cases} 0 & [m = 0, 1, 2, \dots, N - 2] \\ 1 & [m = N - 1] \end{cases}. \quad (9)$$

Although such identity is certainly well-known in the theory of symmetric functions, it does not seem to appear explicitly in such a form in the standard textbooks, such as [56], so we present its proof in Appendix A for the convenience of the reader. Using Eq. (9) in the binomial expansion of Eq. (8), one can see that z_k never has an exponent greater than $N - 2$ and hence the pdf goes to zero. Therefore, the row sums fully govern the support of allowed eigenvalues as

$$\min(z_1, z_2, \dots, z_N) < \lambda < \max(z_1, z_2, \dots, z_N). \quad (10)$$

Moreover, with the help of this identity the normalisation of $P_{\mathbf{z},N}(\lambda)$ can be easily demonstrated, since

$$\int_0^\infty P_{\mathbf{z},N}(\lambda) d\lambda = \sum_{k=1}^N \frac{z_k^{N-1}}{\prod_{l \neq k} (z_k - z_l)} = 1, \quad (11)$$

implying that the cumulative distribution of the Perron-Frobenius eigenvalue is given by

$$F_{\mathbf{z},N}(\lambda) = 1 - \sum_{k=1}^N \frac{(z_k - \lambda)^{N-1}}{\prod_{l \neq k} (z_k - z_l)} \Theta[z_k - \lambda]. \quad (12)$$

A general expression for the m -th moment of the Perron-Frobenius eigenvalue can be derived for finite N as

$$\langle \lambda^m \rangle = \int_0^\infty P_{\mathbf{z},N}(\lambda) \lambda^m d\lambda = \frac{(N - 1)! m!}{(m + N - 1)!} \sum_{k=1}^N \frac{z_k^{N+m-1}}{\prod_{l \neq k} (z_k - z_l)}. \quad (13)$$

Specialising to $m = 1, 2$ we get for the mean and second moment:

$$\langle \lambda \rangle = \frac{\beta}{N} \quad \text{and} \quad \langle \lambda^2 \rangle = \frac{r^2 + \beta^2}{N(N+1)}, \quad (14)$$

where the quantities $\beta = \sum_i z_i$ and $r^2 = \sum_i z_i^2$ have been introduced, which are both of order N .

In Fig. 1 we compare results of numerical simulations for rank-1 NNEMs of the form in Eq. (1) with the exact pdf $P_{z,N}(\lambda)$ as well as with its Gaussian approximation

$$P(\lambda) \approx \frac{1}{\sqrt{2\pi}} \left(\frac{r^2}{N^2} - \frac{\beta^2}{N^3} \right)^{-1/2} \exp \left[-\frac{\left(\lambda - \frac{\beta}{N} \right)^2}{2 \left(\frac{r^2}{N^2} - \frac{\beta^2}{N^3} \right)} \right], \quad (15)$$

where the variance in the Gaussian approximation is given by

$$\langle \lambda^2 \rangle - \langle \lambda \rangle^2 \approx \frac{r^2}{N^2} - \frac{\beta^2}{N^3}. \quad (16)$$

Note that the second term in the variance is not sub-leading for large N as one might naively conclude, as β^2 is of order N^2 whereas r^2 is only of order N .

In Fig. 1 we show the exact pdf for small N and the large N approximation, with both uniformly and exponentially distributed sets of $\{z_i\}$. These plots are shown with a normalised histogram containing data from numerical simulation of 1,000,000 samples of rank-1 NNEMs of the form in Eq. (1) with different sets of the random variables $\{a_i\}$. The accuracy of Eq. (13) was also tested using numerical simulation by measuring the moments of the non-zero eigenvalue for $N = 10$ matrices with both uniformly and exponentially distributed sets of $\{z_i\}$. This is shown in Table I.

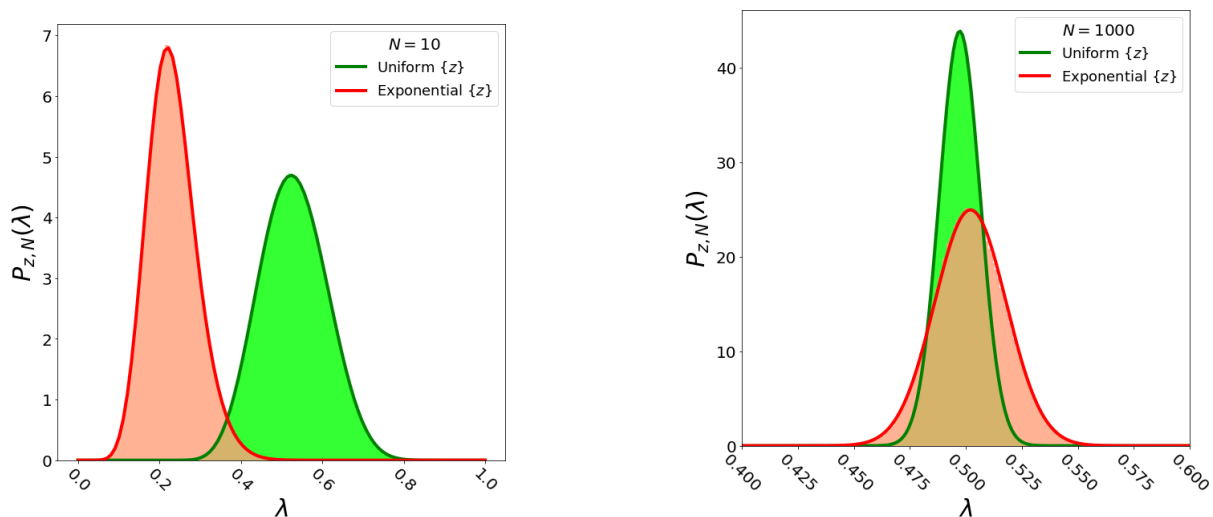


FIG. 1. Probability distribution functions (solid lines) and normalised histograms (shaded regions) generated in numerical simulation of the non-zero eigenvalue of rank-1 NNEMs of the form in Eq. (1). The green plots indicate matrices where the row sums are drawn from a uniform distribution between $[0, 1]$ and the red plots indicate matrices where the row sums are drawn from an exponential distribution with mean 0.5. Left: Solid lines indicate the exact pdf from Eq. (8) for $N = 10$ matrices. Right: solid lines indicate the approximate Gaussian pdf from Eq. (15) for $N = 1000$ matrices. Each normalised histogram contains 1,000,000 samples of eigenvalues observed from numerical simulation of NNEMs of the form in Eq. (1) with different sets of $\{a_i\}$.

B. Non-zero singular value

The non-zero singular value of the matrix T_1 reads

$$\sigma = \sqrt{\left(\sum_{i=1}^N z_i^2 \right) \left(\sum_{i=1}^N a_i^2 \right)} = r \sqrt{\sum_{i=1}^N a_i^2}. \quad (17)$$

m	Exact decimal Eq. (13)	Simulation	m	Exact decimal Eq. (13)	Simulation
0	1.000	1.000	0	1.000	1.000
1	5.293×10^{-1}	5.292×10^{-1}	1	2.322×10^{-1}	2.321×10^{-1}
2	2.868×10^{-1}	2.867×10^{-1}	2	5.758×10^{-2}	5.757×10^{-2}
3	1.590×10^{-1}	1.589×10^{-1}	3	1.518×10^{-2}	1.518×10^{-2}
4	8.998×10^{-2}	8.992×10^{-2}	4	4.233×10^{-3}	4.234×10^{-3}

TABLE I. Comparison between numerical simulation and exact values of $\langle \lambda^m \rangle$ analytically predicted in Eq. (13) for rank-1 NNEMs of the form in Eq. (1). This is tested using $N = 10$ matrices with uniformly distributed sets of $\{z_i\}$ between $[0, 1]$ (left) and exponentially distributed sets of $\{z_i\}$ with mean 0.5 (right). All numerically simulated data is generated as the average of 1,000,000 samples of eigenvalues of rank-1 NNEMs with different sets of $\{a_i\}$.

It is more convenient to evaluate the pdf of its squared value, given by

$$\mathcal{P}_{\mathbf{z},N}(\sigma^2) = C_N \int_0^\infty da_1 \int_0^\infty da_2 \cdots \int_0^\infty da_N \delta\left(\sum_{i=1}^N a_i - 1\right) \delta\left(r^2 \sum_{i=1}^N a_i^2 - \sigma^2\right), \quad (18)$$

where, once again, $C_N = (N-1)!$ is the normalisation constant. Obviously, the pdf of the singular value $\hat{\mathcal{P}}_{\mathbf{z},N}(\sigma)$ is given by $\hat{\mathcal{P}}_{\mathbf{z},N}(\sigma) = (2\sigma/r^2)\mathcal{P}_{\mathbf{z},N}(\sigma^2)$. From the above equation, it is apparent that the distribution of the non-zero singular value squared of the rank-1 random matrix T_1 is closely related to the distribution of the sum of squares of flat Dirichlet random variables.

In spite of the apparent simplicity of this problem, an exact expression for the latter is very cumbersome, and essentially intractable in practice [57, 58]. It is therefore desirable to derive an exact (and computationally fast) expression for the k -th moment of the distribution, as

$$\langle (\sigma^2)^k \rangle = \begin{cases} 1 & [k = 0] \\ r^{2k} \frac{(N-1)!}{(2k+N-1)!} \sum_{\ell=1}^{\min(N,k)} \frac{N!}{(N-\ell)!} B_{k,\ell}(f(1), 2!f(2), \dots, (k-\ell+1)!f(k-\ell+1)) & [k \geq 1] \end{cases}, \quad (19)$$

where $B_{k,\ell}$ are the Bell polynomials and $f(m) = (2m)!/m!$. For details of the derivation of this equation see Appendix B. Table II shows a comparison between results obtained from Eq. (19) and a numerically simulated average of the moments of $\langle (\sigma^2)^k \rangle / r^{2k}$ for rank-1 NNEMs of the form in Eq. (1). One can see from the Table that the equation and simulation agree very well, as expected.

As an exact evaluation of the pdf in Eq. (18) via a double Laplace transformation is challenging to perform, a more fruitful approach is to rewrite the pdf in the form of an iteration with respect to the size of the matrix:

$$\mathcal{P}_{\mathbf{z},N}(\sigma^2, t) \propto \int_D da_N \mathcal{P}_{\mathbf{z},N-1}(\sigma^2 - r^2 a_N^2, t - a_N). \quad (20)$$

In the definition of this iteration \mathbf{z} is a vector of size N , which is used on both sides of the proportionality to define r^2 and, once again, an auxiliary variable t has been introduced such that $\sum_i a_i = t$, which is set to 1 in all final expressions. The integration domain D is defined to be over all values of a_N that satisfy simultaneously the two constraints, both

$$\frac{r^2(t - a_N)^2}{N-1} \leq \sigma^2 - r^2 a_N^2 \leq r^2(t - a_N)^2 \quad \text{and} \quad 0 \leq a_N \leq t. \quad (21)$$

The first constraint arises due to the fact that for N random variables summing to t the sum of squares ranges from t^2/N to t^2 . Hence for an $N \times N$ matrix of the form in Eq. (1) the support of allowed singular values squared is $[r^2/N, r^2]$. The exact form of the pdf can be evaluated for $\mathcal{P}_{\mathbf{z},1}(\sigma^2)$, which, in principle, can be integrated to obtain higher- N pdfs. In Appendix C we use this iterative method to derive the distribution of the non-zero singular value squared for $N = 1, 2$ and 3, which are then validated through numerical simulation. The methods used to iteratively evaluate the distributions are based on the use of a similar method with uniform random variables [59].

In order to understand the large N behaviour of this distribution, it is important to utilise the fact that the constraint on the linear sum of the random variables $\{a_i\}$ becomes weaker as the size of the matrix becomes large.

k	Exact fraction Eq. (19)	Exact decimal Eq. (19)	Simulation
$(N = 10)$ 1	$\frac{2}{11}$	1.818×10^{-1}	1.819×10^{-1}
2	$\frac{5}{143}$	3.497×10^{-2}	3.500×10^{-2}
3	$\frac{36}{5005}$	7.193×10^{-3}	7.203×10^{-3}
4	$\frac{3}{1870}$	1.604×10^{-3}	1.607×10^{-3}
5	$\frac{1909}{4849845}$	3.936×10^{-4}	3.948×10^{-4}

k	Exact fraction Eq. (19)	Exact decimal Eq. (19)	Simulation
$(N = 100)$ 1	$\frac{2}{101}$	1.980×10^{-2}	1.980×10^{-2}
2	$\frac{70}{176851}$	3.958×10^{-4}	3.959×10^{-4}
3	$\frac{643}{80467205}$	7.991×10^{-6}	7.992×10^{-6}
4	$\frac{15650}{95987378947}$	1.630×10^{-7}	1.631×10^{-7}
5	$\frac{286}{84998518181}$	3.365×10^{-9}	3.366×10^{-9}

TABLE II. Comparison between simulation and exact fractional and decimal values of $\langle(\sigma^2)^k\rangle/r^{2k}$ of rank-1 NNEMs with prescribed row sums of the form in Eq. (1). This is shown for a range of k at two fixed values of N (upper table $N = 10$ and lower table $N = 100$), where the sets of row sums are drawn individually from a uniform distribution between $[0, 1]$. These numerical results are independent of the value of r^2 and as such pertain to the moments of the sum of squares of Dirichlet random variables and all rank-1 NNEMs of the form in Eq. (1). All simulated data points are the average over 1,000,000 samples of matrices of the form in Eq. (1) with different sets of $\{a_i\}$.

Eq. (19) can be used to obtain the first and second moments of σ^2 as

$$\langle\sigma^2\rangle = \frac{2r^2}{N+1} \quad \text{and} \quad \langle(\sigma^2)^2\rangle = r^4 \left(\frac{24N!}{(N+3)!} + \frac{4N!(N-1)}{(N+3)!} \right). \quad (22)$$

Using these and invoking the central limit theorem one can infer that the large N pdf must be a Gaussian with mean $2r^2/N$ and variance

$$\langle(\sigma^2)^2\rangle - \langle\sigma^2\rangle^2 = r^4 \left(\frac{24N!}{(N+3)!} + \frac{4N!(N-1)}{(N+3)!} - \frac{4}{(N+1)^2} \right) \approx \frac{4r^4}{N^3}, \quad (23)$$

such that

$$\mathcal{P}_{\mathbf{z},N}(\sigma^2) \approx \sqrt{\frac{N^3}{8\pi r^4}} \exp\left(-\frac{N^3}{8r^4} \left(\sigma^2 - \frac{2r^2}{N}\right)^2\right). \quad (24)$$

Fig. 2 shows a comparison between the large N pdf in Eq. (24) and normalised histograms of numerically generated samples of the non-zero singular value squared of large rank-1 NNEMs of the form in Eq. (1). This is demonstrated for two different values of N , where the sets of $\{z_i\}$ are drawn from a uniform distribution between $[0, 1]$. From these comparisons, one can see that the approximation becomes more accurate at higher values of N and describes the distribution of the square of the non-zero singular value well.

III. ONE-PARAMETER FAMILY OF RANK-2 NNEMS

In general, an $N \times N$ rank-2 matrix can be constructed as the sum of two rank-1 matrices, such that

$$M_2 = \mathbf{x}\mathbf{a}^T + \mathbf{y}\mathbf{b}^T, \quad (25)$$

where \mathbf{x} , \mathbf{a} , \mathbf{y} and \mathbf{b} are N -dimensional vectors. In this Section, we consider the statistical properties of the eigenvalues and singular values of a simple rank-2 matrix with non-negative entries. This so-called one-parameter family of rank-2 NNEMs has a single random variable which we perform averages over. In addition to prescribed sums of the elements

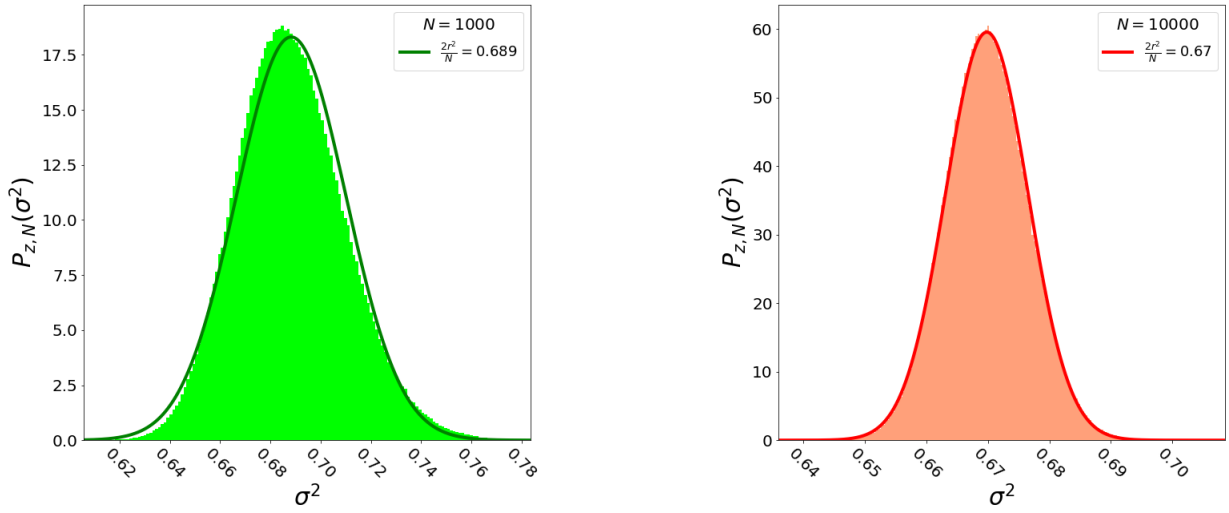


FIG. 2. Probability distribution functions (solid lines) and normalised histograms (shaded regions) generated in numerical simulation of the non-zero singular value squared for large rank-1 NNEMs of the form in Eq. (1), left: $N = 1000$ and right: $N = 10000$. In both plots the solid line is the approximate Gaussian pdf generated using Eq. (24) and the sets of $\{z_i\}$ are drawn from a uniform distribution between $[0, 1]$. One can see that the agreement between the theoretical pdfs and the normalised histograms generated in numerical simulation is stronger for the higher value of N in the right-hand plot. Each histogram consists of 1,000,000 numerically generated samples of the non-zero singular value with different sets of $\{a_i\}$.

in each row, this family of matrices also has prescribed sums of the elements in each column. Thus matrices within this family have $2N$ prescribed macroscopic quantities (all row and column sums) whilst still being a random matrix, a feat which cannot be achieved for rank-1 matrices.

This class of rank-2 NNEMs is obtained as an extension of the rank-1 NNEMs of the form in Eq. (1). Specifically, the elements in the first $N - 1$ columns are perturbed in a different way from the elements in the N th column. This is done through the use of a single random variable ϵ , in the following way

$$T_2 = \begin{pmatrix} a_1(z_1 - \epsilon) & a_2(z_1 - \epsilon) & \dots & a_{N-1}(z_1 - \epsilon) & a_N(z_1 - \epsilon) + \epsilon \\ a_1(z_2 - \epsilon) & a_2(z_2 - \epsilon) & \dots & a_{N-1}(z_2 - \epsilon) & a_N(z_2 - \epsilon) + \epsilon \\ \vdots & \vdots & \ddots & \vdots & \vdots \\ a_1(z_N - \epsilon) & a_2(z_N - \epsilon) & \dots & a_{N-1}(z_N - \epsilon) & a_N(z_N - \epsilon) + \epsilon \end{pmatrix}. \quad (26)$$

This matrix can also be expressed as the sum of two rank-1 matrices, as in Eq. (25), using the following vectors

$$\mathbf{x} = \begin{pmatrix} z_1 - \epsilon \\ z_2 - \epsilon \\ \vdots \\ z_N - \epsilon \end{pmatrix}, \quad \mathbf{a} = \begin{pmatrix} a_1 \\ a_2 \\ \vdots \\ a_N \end{pmatrix}, \quad \mathbf{y} = \begin{pmatrix} 1 \\ 1 \\ \vdots \\ 1 \end{pmatrix}, \quad \mathbf{b} = \begin{pmatrix} 0 \\ 0 \\ \vdots \\ \epsilon \end{pmatrix}. \quad (27)$$

The elements in column i of matrices within this family can be prescribed to sum to ζ_i , if one chooses the variables a_i as

$$a_i = \begin{cases} \frac{\zeta_i}{\beta - N\epsilon} & [i \neq N] \\ \frac{\zeta_N - N\epsilon}{\beta - N\epsilon} & [i = N] \end{cases}, \quad (28)$$

such that they only depend on the random variable ϵ . For rank-2 matrices with prescribed column and row sums, one must extend the definition of β such that

$$\beta = \sum_{i=1}^N z_i = \sum_{i=1}^N \zeta_i, \quad (29)$$

which is equivalent to the sum over all elements in the matrix. In this regime, the only random variable is ϵ as each a_i only depends on ϵ . The values of a_i described in Eq. (28) still maintain the condition that the sum over all a_i s is equal to 1, since

$$\sum_{i=1}^N a_i = \frac{\sum_{i=1}^N \zeta_i - N\epsilon}{\beta - N\epsilon} = \frac{\beta - N\epsilon}{\beta - N\epsilon} = 1, \quad (30)$$

hence the sum of the elements in row i is still prescribed as z_i . Maintaining this setup but choosing $\epsilon = 0$ yields a rank-1 NNEM where all row and column sums are fixed, but the elements are not random.

In order to ensure that all the entries of rank-2 matrices within this class are non-negative, the following conditions must be met (i) $z_i - \epsilon \geq 0$ and (ii) $a_N(z_i - \epsilon) + \epsilon \geq 0$ for all i . The first of these conditions ensures that all elements in the first $N - 1$ columns are non-negative as the denominator in each a_i , $\beta - N\epsilon$, is also constrained to be non-negative, since

$$\beta = \sum_{i=1}^N z_i \geq \sum_{i=1}^N \epsilon = N\epsilon. \quad (31)$$

The second condition leads to slightly more complicated constraints. To find the value of ϵ where the entry in the i th row of the N th column goes to zero we set condition (ii) to zero and use the definition of a_N given in Eq. (28), this gives a set of critical values of ϵ as

$$\epsilon_i(z_i) = \frac{z_i \zeta_N}{N z_i + \zeta_N - \beta}. \quad (32)$$

The value of $\epsilon_i(z_i)$ can be both positive and negative depending on the nature of the prescribed sets of $\{z_i\}$ and $\{\zeta_i\}$, specifically this depends on the sign of $N z_i + \zeta_N - \beta$. In order to ensure that all entries are non-negative, strict constraints must be placed on the values of ϵ , i.e. when $\epsilon_i \leq 0$ then we must choose $\epsilon \geq \epsilon_i$ and vice versa when $\epsilon_i \geq 0$. Conditions (i) and (ii) lead to $2N$ inequalities on the value that ϵ can take, therefore, in order to determine the limits on the value of ϵ , the smallest and largest of these inequalities must be determined.

Considering the positive constraints first of all, the smallest of these will be given by $\epsilon \leq z_{\min}$ or $\epsilon \leq \epsilon_i(z_{\max})$, where z_{\min} and z_{\max} are the smallest and largest row sums respectively. With regards to the negative constraints, the largest of these will be given by $\epsilon \leq \epsilon_i(z_{\min})$, if this value is negative. However, if this value is non-negative then there will be no lower limit on the value of ϵ . This rare but interesting case occurs when $N z_i + \zeta_N - \beta > 0$ for all i , or more specifically $N z_{\min} + \zeta_N - \beta > 0$. Hence, we can say that in order to produce NNEMs then ϵ must be within $\epsilon_{\min} \leq \epsilon \leq \epsilon_{\max}$, where

$$\epsilon_{\max} = \min \left(z_{\min}, \frac{z_{\max} \zeta_N}{N z_{\max} + \zeta_N - \beta} \right) \quad (33)$$

and

$$\epsilon_{\min} = \begin{cases} \frac{z_{\min} \zeta_N}{N z_{\min} + \zeta_N - \beta} & [N z_{\min} + \zeta_N - \beta < 0] \\ -\infty & [N z_{\min} + \zeta_N - \beta \geq 0] \end{cases}. \quad (34)$$

One should note that for the vast majority of matrices the value of ϵ_{\min} is negative and finite. These are the matrices whose spectral properties we will mostly focus on.

With the definition of this family of matrices now in place, we will now analyse some of its spectral properties. Namely, in the next two subsections we will consider the distribution of the sum and product of the eigenvalues and singular values. Then, we consider the spectral properties in the limit of large negative ϵ and the different limits in which this one-parameter family of rank-2 matrices can be reduced to being rank-1. Following that, in Sec. IV, we present results pertaining to the resolvent vector of this class of rank-2 matrices.

A. Non-zero eigenvalues

Rank-2 matrices have two non-zero eigenvalues and these can be expressed as

$$\lambda_{1,2} = \frac{T}{2} \pm \frac{1}{2} \sqrt{T^2 - 4D} \quad (35)$$

respectively, where the values of T and D are given below. Clearly

$$T = \lambda_1 + \lambda_2 \quad \text{and} \quad D = \lambda_1 \lambda_2 . \quad (36)$$

For the case of a general rank-2 matrix, as in Eq. (25), the non-zero eigenvalues are described fully by

$$T = \text{Tr}(M_2) = \mathbf{x} \cdot \mathbf{a} + \mathbf{y} \cdot \mathbf{b} \quad (37)$$

and

$$D = \sum_{i < j} \det \begin{pmatrix} a_i & b_i \\ a_j & b_j \end{pmatrix} \det \begin{pmatrix} x_i & y_i \\ x_j & y_j \end{pmatrix} . \quad (38)$$

Specialising these relationships to the vectors \mathbf{x} , \mathbf{a} , \mathbf{y} and \mathbf{b} that define the one-parameter family of rank-2 matrices described in Eqs. (26) and (27), one may express T and D in terms of the random variable ϵ and some matrix specific quantities, such that

$$T(\epsilon) = \frac{\alpha - Nz_N \epsilon}{\beta - N\epsilon} \quad \text{and} \quad D(\epsilon) = \frac{\epsilon(\alpha - z_N \beta)}{\beta - N\epsilon} , \quad (39)$$

where the quantity

$$\alpha = \sum_{i=1}^N \zeta_i z_i , \quad (40)$$

has been introduced and $\beta = \sum_i z_i = \sum_i \zeta_i$ as before.

We will now compute the marginal probability densities of the sum and product of the two non-zero eigenvalues, assuming that the only randomness in the model arises from ϵ , which we draw from a uniform distribution between ϵ_{\min} and ϵ_{\max} . To begin with, the distribution of the sum of the eigenvalues is derived starting from

$$P(T) = C_\epsilon \int_{\epsilon_{\min}}^{\epsilon_{\max}} d\epsilon \delta \left(T - \frac{\alpha - Nz_N \epsilon}{\beta - N\epsilon} \right) , \quad (41)$$

where the normalisation constant C_ϵ is defined as

$$C_\epsilon = \frac{1}{\epsilon_{\max} - \epsilon_{\min}} . \quad (42)$$

Carrying out the integration, we find that

$$P(T) = C_\epsilon \begin{cases} \frac{|\alpha - z_N \beta|}{N(T - z_N \beta)^2} & [T_{\min} \leq T \leq T_{\max}] \\ 0 & [\text{otherwise}] \end{cases} , \quad (43)$$

where

$$T_{\min} = \begin{cases} T(\epsilon_{\min}) \\ T(\epsilon_{\max}) \end{cases} \quad T_{\max} = \begin{cases} T(\epsilon_{\max}) & [\alpha > z_N \beta] \\ T(\epsilon_{\min}) & [\alpha < z_N \beta] \end{cases} . \quad (44)$$

Additionally, by following a similar method, the distribution of the product of the two non-zero eigenvalues can be derived as

$$P(D) = C_\epsilon \begin{cases} \frac{\beta |\alpha - z_N \beta|}{(DN + \alpha - z_N \beta)^2} & [D_{\min} \leq D \leq D_{\max}] \\ 0 & [\text{otherwise}] \end{cases} , \quad (45)$$

where

$$D_{\min} = \begin{cases} D(\epsilon_{\min}) \\ D(\epsilon_{\max}) \end{cases} \quad D_{\max} = \begin{cases} D(\epsilon_{\max}) & [\alpha > z_N \beta] \\ D(\epsilon_{\min}) & [\alpha < z_N \beta] \end{cases} . \quad (46)$$

The dependence of the end-points of the support on the sign of $\alpha - z_N \beta$ can be seen explicitly by considering the first derivative of both $T(\epsilon)$ and $D(\epsilon)$. In both cases the sign of the derivative, within the support of allowed values of ϵ , purely depends on the sign of $\alpha - z_N \beta$.

In Fig. 3 we plot the distributions of the sum and product of the non-zero eigenvalues of rank-2 matrices generated according to Eq. (26). Each plot contains a solid line representing a theoretical pdf generated from the equations derived above, as well as a normalised histogram of values obtained from a sample of 1,000,000 numerically generated rank-2 NNEMs within the one-parameter family described by Eq. (26).

One can also derive exact expressions for the pdfs of the individual eigenvalues and the spectral gap as well as the joint probability density of the sum and product of the eigenvalues, these expressions can be found in Appendix D.

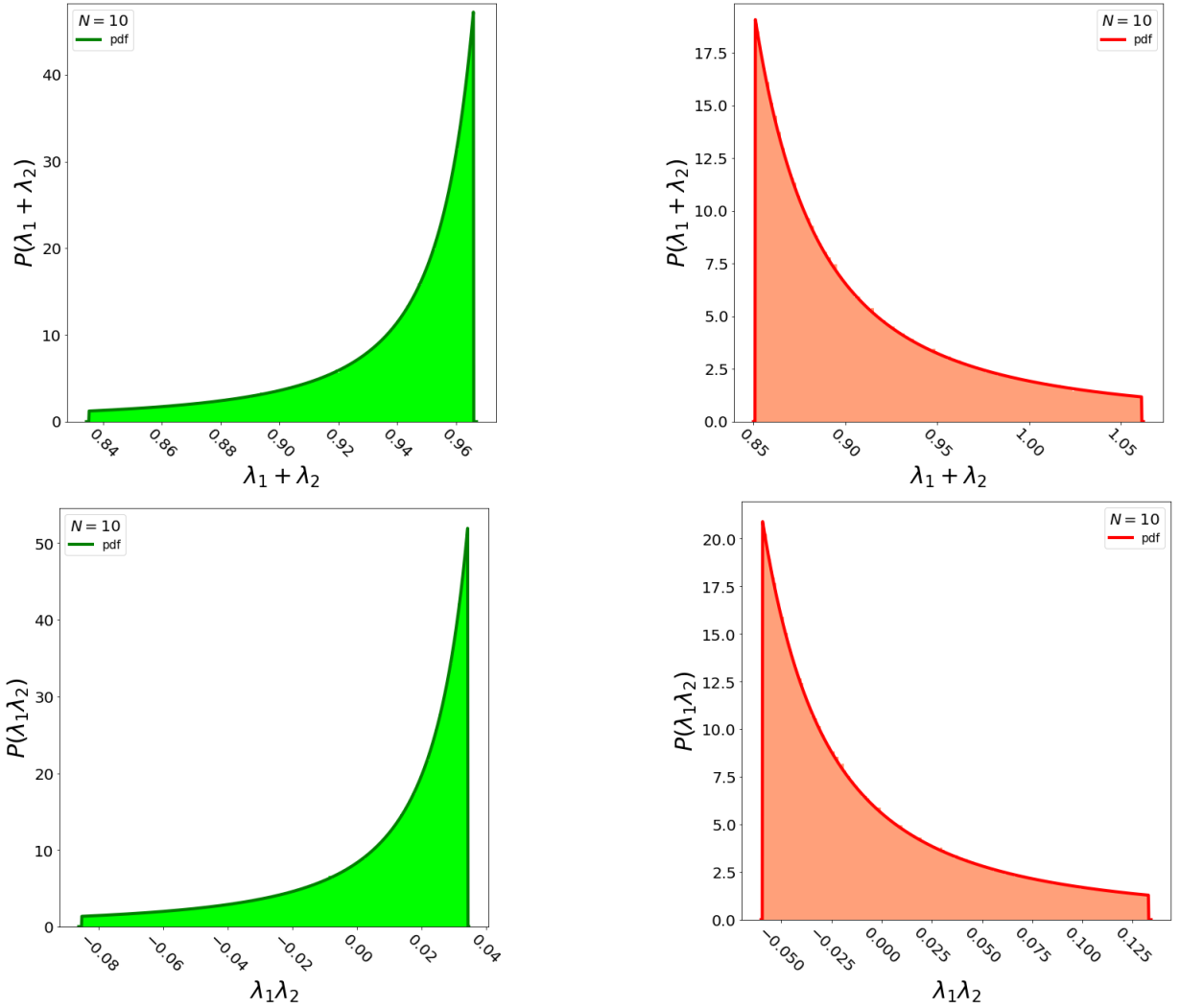


FIG. 3. Probability density functions of the sum and product of the non-zero eigenvalues of matrices within the one-parameter family of rank-2 NNEMs of the form in Eq. (26). The green plots on the left-hand side indicate matrices with $\alpha < z_N \beta$ whereas the red plots on the right-hand side indicate matrices with $\alpha > z_N \beta$. Top: plots of the pdf of $T = \lambda_1 + \lambda_2$. Bottom: plots of the pdf of $D = \lambda_1 \lambda_2$. Each plot contains a theoretical pdf (solid line) and a normalised histogram (shaded region) of 1,000,000 values observed in numerical simulation of $N = 10$ rank-2 NNEMs of the form in Eq. (26). Note how the plots appear to mirror each other. The fixed row and column sums are generated by observing the row and column sums of a substochastic matrix created by removing a random row and column, of the same index, from an original row-stochastic matrix of size $N + 1 \times N + 1$. The entries of each independent row of the original stochastic matrix were drawn as the elements of a flat Dirichlet random vector.

B. Non-zero singular values

Similarly, a rank-2 matrix will possess two non-zero singular values. The square of these singular values can be formulated as

$$\sigma_{1,2}^2 = \frac{\tau}{2} \pm \frac{1}{2} \sqrt{\tau^2 - 4\Delta}, \quad (47)$$

such that their sum and product are given by

$$\tau = \sigma_1^2 + \sigma_2^2 \quad \text{and} \quad \Delta = \sigma_1^2 \sigma_2^2, \quad (48)$$

respectively. Once again, one can write down equations that fully describe the non-zero singular values for a general rank-2 matrix, as in Eq. (25), as

$$\tau = \text{Tr}(M_2^T M_2) = \sum_{i,j}^N (x_i a_j + y_i b_j)^2 \quad (49)$$

and

$$\Delta = \left(\sum_{i < j} \det \begin{pmatrix} a_i & b_i \\ a_j & b_j \end{pmatrix} \right)^2 \left(\sum_{k < l} \det \begin{pmatrix} x_k & y_k \\ x_l & y_l \end{pmatrix} \right)^2. \quad (50)$$

Using the definitions of \mathbf{x} , \mathbf{a} , \mathbf{y} and \mathbf{b} from Eq. (27), the values of τ and Δ , for rank-2 matrices within the one-parameter family described by Eq. (26), can be expressed in terms of ϵ and some new matrix specific quantities, such that

$$\tau(\epsilon) = \frac{r^2 R^2 + A\epsilon + B\epsilon^2}{(\beta - N\epsilon)^2} \quad \text{and} \quad \Delta(\epsilon) = (R^2 - \zeta_N^2) \kappa \frac{\epsilon^2}{(\beta - N\epsilon)^2}, \quad (51)$$

where

$$R^2 = \sum_{i=1}^N \zeta_i^2 \quad (52)$$

$$\kappa = Nr^2 - \beta^2 = \sum_{i < j} (z_i - z_j)^2 \quad (53)$$

$$A = -2(\kappa\zeta_N + R^2\beta) \quad (54)$$

$$B = N(\kappa + R^2). \quad (55)$$

From the above definitions, one can note that for NNEMs (where all z_i and ζ_i are non-negative) the above constants have definite signs, i.e. $R^2 \geq 0$, $\kappa \geq 0$, $A \leq 0$ and $B \geq 0$. In a similar way to the previous subsection, we now compute the marginal probability densities of the sum and product of the two non-zero squared singular values. In doing so, we assume that the only randomness in the model arises from ϵ , which, once again, we draw from a uniform distribution between ϵ_{\min} and ϵ_{\max} . The expression for the pdf of the sum of the non-zero squared singular values must be derived starting from the integral,

$$P(\tau) = C_\epsilon \int_{\epsilon_{\min}}^{\epsilon_{\max}} d\epsilon \delta \left(\tau - \frac{r^2 R^2 + A\epsilon + B\epsilon^2}{(\beta - N\epsilon)^2} \right). \quad (56)$$

This can be carefully evaluated to give the distribution

$$P(\tau) = C_\epsilon \begin{cases} 0 & [\tau < \tau_{\min}] \\ \mathcal{P}_+(\tau) + \mathcal{P}_-(\tau) & [\tau_{\min} \leq \tau \leq \tau'] \\ \Theta[\tau(\epsilon_{\min}) - \tau(\epsilon_{\max})] \mathcal{P}_+(\tau) + \Theta[\tau(\epsilon_{\max}) - \tau(\epsilon_{\min})] \mathcal{P}_-(\tau) & [\tau' < \tau \leq \tau_{\max}] \\ 0 & [\tau > \tau_{\max}] \end{cases}, \quad (57)$$

where the functions $\mathcal{P}_\pm(\tau)$ are defined as

$$\mathcal{P}_\pm(\tau) = \frac{N^2}{4(B - N^2\tau)^2} \frac{(2\kappa(\beta - \zeta_N) \pm \gamma(\tau))^2}{\gamma(\tau)}, \quad (58)$$

such that

$$\gamma(\tau) = \sqrt{4(\beta AN + B\beta^2 + N^2 r^2 R^2)\tau + A^2 - 4r^2 R^2 B}. \quad (59)$$

The significant values of τ in this support are given by

$$\tau_{\min} = \begin{cases} \tau(\epsilon_s) & [\epsilon_{\min} < \epsilon_s < \epsilon_{\max}] \\ \min[\tau(\epsilon_{\min}), \tau(\epsilon_{\max})] & [\text{otherwise}] \end{cases} \quad (60)$$

$$\tau' = \min[\tau(\epsilon_{\min}), \tau(\epsilon_{\max})] \quad (61)$$

$$\tau_{\max} = \max[\tau(\epsilon_{\min}), \tau(\epsilon_{\max})] \quad (62)$$

with

$$\epsilon_s = -\frac{1}{N} \frac{R^2 - \zeta_N \beta}{\beta - \zeta_N} \quad \text{and} \quad \tau(\epsilon_s) = -\frac{A^2 - 4r^2 R^2 B}{4(\beta A N + B\beta^2 + r^2 R^2 N^2)}, \quad (63)$$

such that $(\epsilon_s, \tau(\epsilon_s))$ are the coordinates of the minimum of the function $\tau(\epsilon)$.

Similarly, to evaluate the pdf of the product of the non-zero singular values squared, we begin from

$$P(\Delta) = C_\epsilon \int_{\epsilon_{\min}}^{\epsilon_{\max}} d\epsilon \delta\left(\Delta - (R^2 - \zeta_N^2) \kappa \frac{\epsilon^2}{(\beta - N\epsilon)^2}\right). \quad (64)$$

This integration can be carefully carried out to give

$$P(\Delta) = C_\epsilon \begin{cases} 0 & [\Delta < 0] \\ P_+(\Delta) + P_-(\Delta) & [0 \leq \Delta \leq \Delta'] \\ \Theta[\Delta(\epsilon_{\max}) - \Delta(\epsilon_{\min})]P_+(\Delta) + \Theta[\Delta(\epsilon_{\min}) - \Delta(\epsilon_{\max})]P_-(\Delta) & [\Delta' < \Delta \leq \Delta_{\max}] \\ 0 & [\Delta > \Delta_{\max}] \end{cases}, \quad (65)$$

with contributing functions

$$P_\pm(\Delta) = \frac{\beta}{2\Delta} \sqrt{\frac{(R^2 - \zeta_N^2)\kappa}{\Delta}} \frac{1}{\left(N \pm \sqrt{(R^2 - \zeta_N^2)\frac{\kappa}{\Delta}}\right)^2}, \quad (66)$$

and key-points in the spline defined as

$$\Delta_{\max} = \max[\Delta(\epsilon_{\min}), \Delta(\epsilon_{\max})] \quad (67)$$

$$\Delta' = \min[\Delta(\epsilon_{\min}), \Delta(\epsilon_{\max})]. \quad (68)$$

Note that the smallest value of Δ that is allowed is $\Delta = 0$. This is because the point where $\Delta(\epsilon = 0) = 0$ is a global minimum of $\Delta(\epsilon)$ and $\epsilon = 0$ will always be in the support of allowed values of ϵ .

There are two functions $\mathcal{P}_\pm(\tau)$ and $P_\pm(\Delta)$ that contribute to both the pdfs of τ and Δ respectively. This interplay between two different functions arises because the arguments of the δ function in Eqs. (56) and (64) can have two possible roots in terms of ϵ , which may or may not be within the support of allowed values. This is the reason why the pdfs are expressed as discontinuous spline functions, as when $\tau = \tau'$ or $\Delta = \Delta'$, the number of solutions within the support of ϵ changes from two to one, resulting in a discontinuity in the pdf. Note that, for the distribution of τ , when ϵ_s is not within the support of ϵ , the discontinuity is not seen within the distribution. Whereas, for the distribution of Δ the discontinuity will always be present.

In Fig. 4 we show examples of the pdfs of the sum and product of the non-zero squared singular values of $N = 10$ rank-2 NNEMs of the form in Eq. (26) (in semi-log scale). From this Figure, one can observe the discontinuity in the probability density at τ' and Δ' . In order to distinguish between distributions where the plus or minus solutions contribute after the discontinuity, we introduce the following quantities

$$\tau_R = \tau(\epsilon_{\max}) - \tau(\epsilon_{\min}) \quad \text{and} \quad \Delta_R = \Delta(\epsilon_{\max}) - \Delta(\epsilon_{\min}). \quad (69)$$

C. The limit of large negative ϵ and reduction to rank-1

As mentioned earlier on in this Section, for matrices satisfying the condition

$$N z_{\min} + \zeta_N - \beta > 0, \quad (70)$$

there is no lower limit on the value of ϵ . Therefore, a natural question to ask about these matrices, is how do they behave in the limit of large negative ϵ ? To learn more about this limit, we first consider how the entries behave and one finds that, in the limit $\epsilon \rightarrow -\infty$, the entries in the first $N - 1$ columns tend to

$$(T_2)_{i,j < N} = \frac{\zeta_j(z_i + |\epsilon|)}{\beta + N|\epsilon|} \rightarrow \frac{\zeta_j}{N}, \quad (71)$$

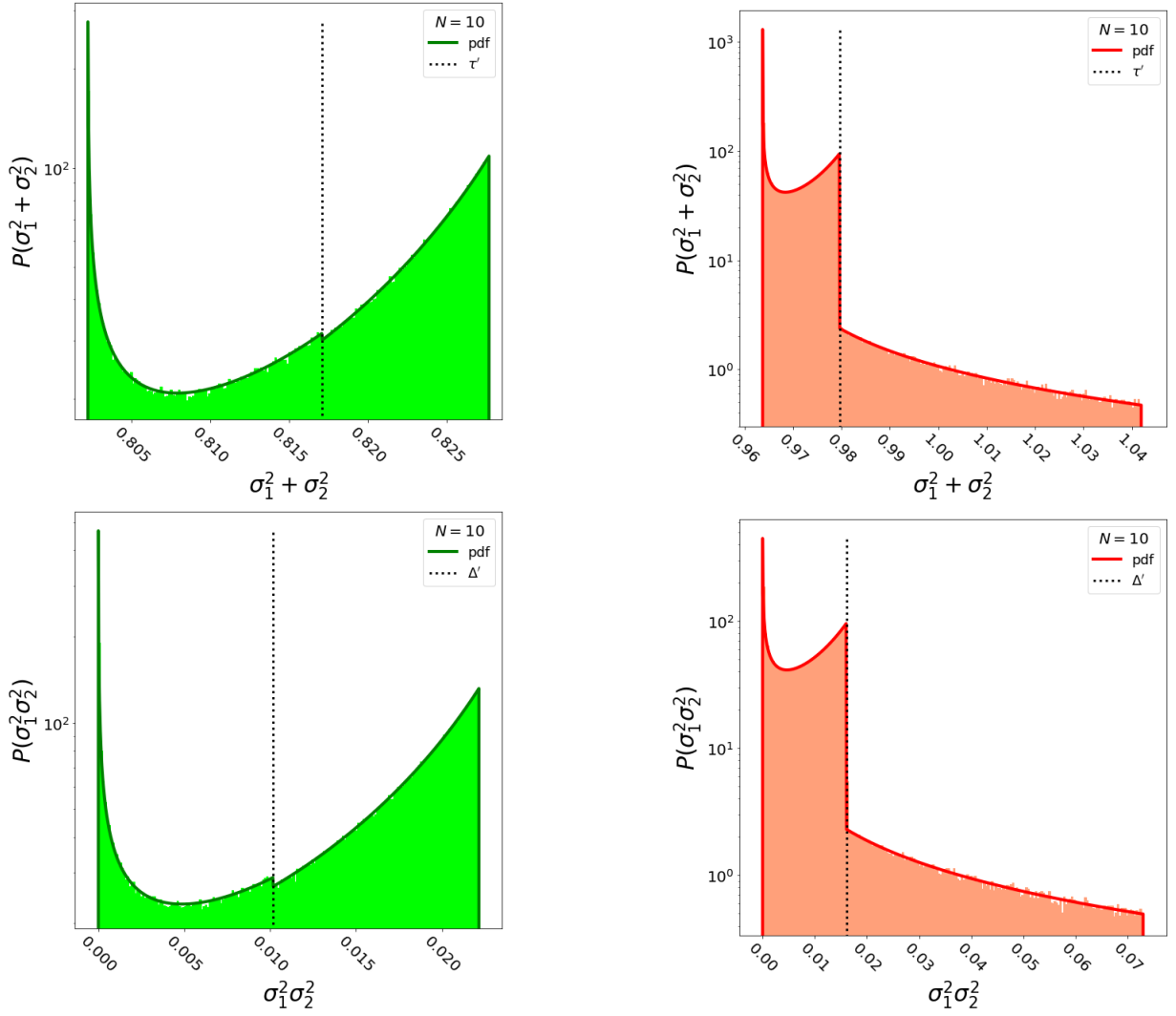


FIG. 4. Probability density functions of the sum and product of the two non-zero squared singular values of matrices within the one-parameter family of rank-2 NNEMs, of the form in Eq. (26). Note that the scale on the y -axis is logarithmic. Top: plots of the pdf of $\tau = \sigma_1^2 + \sigma_2^2$, Bottom: plots of the pdf of $\Delta = \sigma_1^2 \sigma_2^2$. Left hand plots are such that τ_R and $\Delta_R < 0$ and right hand plots are such that τ_R and $\Delta_R > 0$. Each plot contains a theoretical pdf (solid line) and a normalised histogram (shaded region) of 1,000,000 sets of singular values obtained from numerical simulation of $N = 10$ rank-2 NNEMs of the form in Eq. (26). The plots also contain a dotted line that indicates the predicted values of τ' and Δ' , which coincide with the discontinuities in the pdf. The fixed row and column sums are generated by observing the row and column sums of a substochastic matrix created by removing a random row and column, of the same index, from an original row-stochastic matrix of size $N + 1 \times N + 1$. The entries of each independent row of the original stochastic matrix were drawn as the elements of a flat Dirichlet random vector.

whereas the entries in the N th column tend to

$$(T_2)_{i,N} = \frac{(\zeta_N + N|\epsilon|)(z_i + |\epsilon|)}{\beta + N|\epsilon|} - |\epsilon| \rightarrow z_i + \frac{\zeta_N - \beta}{N}. \quad (72)$$

One can easily verify that the condition in Eq. (70) guarantees that all entries are still non-negative and that the sum of the elements in row and column i are still prescribed as z_i and ζ_i respectively. In this limit of large negative ϵ , the distribution of all properties of the eigenvalues and singular values go to sharply-peaked functions around fixed values based on macroscopic quantities of the matrix. Specifically,

$$\lim_{\epsilon \rightarrow -\infty} T = z_N \quad (73)$$

$$\lim_{\epsilon \rightarrow -\infty} D = \frac{1}{N}(z_N \beta - \alpha) \quad (74)$$

$$\lim_{\epsilon \rightarrow -\infty} G = \sqrt{z_N^2 - \frac{4(z_N\beta - \alpha)}{N}} \quad (75)$$

$$\lim_{\epsilon \rightarrow -\infty} \lambda_{1,2} = \frac{z_N}{2} \pm \frac{1}{2} \sqrt{z_N^2 - \frac{4(z_N\beta - \alpha)}{N}} \quad (76)$$

$$\lim_{\epsilon \rightarrow -\infty} \tau = \frac{B}{N^2} \quad (77)$$

$$\lim_{\epsilon \rightarrow -\infty} \Delta = \frac{(R^2 - \zeta_N^2)\kappa}{N^2}, \quad (78)$$

where we have used $G = \lambda_1 - \lambda_2$ to denote the spectral gap.

It is important to note for consistency that the limiting values that the above quantities attain in the limit of large negative ϵ correspond to singularities in the pdfs of the same quantities. For example, if one considers the pdf of T given by Eq. (43), a singularity in the function at $T = z_N$ becomes apparent. The same argument can be applied when considering the pdfs of D , G , $\lambda_{1,2}$, τ and Δ .

Finally, it is also interesting to consider the limits in which this one-parameter family of rank-2 matrices possesses only one non-zero eigenvalue or singular value. As mentioned earlier, this happens trivially in the limit of $\epsilon = 0$ as matrices of the form in Eq. (26) reduce in rank and become identical to the rank-1 matrix in Eq. (1). One can also see that when $\alpha = z_N\beta$ there will only be one non-zero eigenvalue, which is given by $\lambda_1 = z_N$. This case does not yield a reduction in rank as the vector space formed by the columns is still of dimension 2. Additionally, matrices of the form in Eq. (26) will only have one non-zero singular value when $\Delta = 0$, this can happen in three different scenarios: $\epsilon = 0$, $R^2 = \zeta_N^2$ and $\kappa = 0$. It can be easily shown that all of these cases yield true rank-1 NNEMs. Hence, for the one-parameter family of rank-2 NNEMs described by Eq. (26), it is possible to observe a rank-2 matrix with one non-zero eigenvalue but it is not possible to observe a rank-2 matrix with one non-zero singular value.

IV. RESOLVENT STATISTICS OF RANK-1 AND RANK-2 NNEMs

The resolvent $G(T)$ of the matrix T , defined as

$$G(T) = (\mathbf{1} - T)^{-1}, \quad (79)$$

with $\mathbf{1}$ being the $N \times N$ identity matrix, and in particular, the resolvent vector

$$\mathbf{m}(T) = G(T)\mathbf{1}, \quad (80)$$

where $\mathbf{1} = (1, 1, \dots, 1)^T$ is a column vector of all ones, are important in many applications, such as calculation of the Mean First Passage Time (MFPT) of random walks on networks [35, 60, 61], influence of nodes in a complex network [54] and Leontief's input-output multipliers [9, 18].

We recall that MFPT naturally arises in the exploration of complex networks via random walks. It is defined as the average time taken by a random walker to reach a target node j , given that they started at a source node i . If one considers a network of $N + 1$ nodes with normalised transition probabilities between all pairs of nodes i and j , then for a given target node j , the vector of MFPTs from all source nodes is given by $\mathbf{m}(T^{(j)})$. Note that $T^{(j)}$ is an $N \times N$ substochastic matrix formed by removing row j and column j of the target node from the original row-stochastic matrix of normalised transition probabilities. Other applications of $\mathbf{m}(T)$ arise when considering the most "influential" nodes in a network (for example, using the Katz centrality as the relevant metric) [35, 62]. This has many applications in the field of theoretical ecology and the ranking of webpages based on links to other important pages [63, 64]. See also [3] for an in-depth review of the uses of the object in Eq. (80).

In this Section, we present results describing the resolvent vector entries of (i) the random rank-1 approximation with prescribed row sums in Eq. (1) and (ii) the random one-parameter family of rank-2 NNEMs described by Eq. (26). Finally, when considering approximations to general rank- N matrices and substochastic matrices of the form used when computing the MFPT, we make comparisons between the resolvent statistics of these two approximations and a low-rank approximation developed in [35].

A. Rank-1 NNEMs

Considering rank-1 NNEMs of the form in Eq. (1) we can evaluate Eqs. (79) and (80) to determine $G(T_1)$ and $\mathbf{m}(T_1)$. Under the assumption that T_1 has random entries as per Eq. (1), it is therefore an important question

to characterise the joint probability density $P_{\mathbf{z}}(m_1, \dots, m_N)$ of the \mathbf{m} -vector entries. Using the Sherman-Morrison formula [65] for the inverse of a rank-1 matrix, we get

$$m_j = 1 + \frac{z_j}{1 - \sum_k a_k z_k}, \quad (81)$$

therefore

$$P_{\mathbf{z}}(m_1, \dots, m_N) = C_N \int_0^\infty da_1 \cdots \int_0^\infty da_N \delta\left(\sum_{i=1}^N a_i - 1\right) \prod_{j=1}^N \delta\left(m_j - 1 - \frac{z_j}{1 - \sum_k a_k z_k}\right), \quad (82)$$

which can be rewritten in terms of the pdf of the Perron-Frobenius eigenvalue as

$$P_{\mathbf{z}}(m_1, \dots, m_N) = \int_0^\infty d\lambda P_{\mathbf{z},N}(\lambda) \prod_{j=1}^N \delta\left(m_j - 1 - \frac{z_j}{1 - \lambda}\right). \quad (83)$$

An even more interesting quantity is the one-point marginal density $\rho_{\mathbf{z}}(m) = \langle (1/N) \sum_i \delta(m - m_i) \rangle$, where the average is taken w.r.t. the joint pdf in Eq. (83). Skipping details, the analytical formula for the one-point marginal density is given by

$$\rho_{\mathbf{z}}(m) = \frac{N-1}{N} \sum_{i,k} \prod_{l \neq k} \left[\frac{1}{(z_k - z_l)} \right] \left(z_k + \frac{z_i}{m-1} - 1 \right)^{N-2} \frac{z_i}{(m-1)^2} \Theta \left[z_k + \frac{z_i}{m-1} - 1 \right]. \quad (84)$$

For a given pair of i and k , the Θ functions are non-zero between 1 and $1 + z_i/(1 - z_k)$, thus the largest allowed value of m is $1 + z_{\max}/(1 - z_{\max})$. However, if one considers Eq. (81), then it can be seen that the smallest allowed value of m is $1 + z_{\min}/(1 - z_{\min})$, indeed $\rho_{\mathbf{z}}(m)$ goes to zero for all values of $m < 1 + z_{\min}/(1 - z_{\min})$. This can be seen by considering Eq. (84) in the limit where all the Θ functions go to 1 and invoking the use of the identity relating to symmetric functions in Eq. (9). From this analysis of the support of the distribution of m , one can confirm that $\rho_{\mathbf{z}}(m)$ is properly normalised over the support of allowed values

$$1 + \frac{z_{\min}}{1 - z_{\min}} < m < 1 + \frac{z_{\max}}{1 - z_{\max}}. \quad (85)$$

In addition to this, one can also perform the average over the large N limit of the pdf derived in Eq. (15) to obtain an accurate large N approximation to the one-point marginal density as

$$\rho_{\mathbf{z}}(m) = \frac{1}{\sqrt{2\pi N}} \left(\frac{r^2}{N^2} - \frac{\beta^2}{N^3} \right)^{-1/2} \sum_{i=1}^N \frac{z_i}{(m-1)^2} \exp \left[-\frac{\left(1 - \frac{z_i}{(m-1)} - \frac{\beta}{N} \right)^2}{2 \left(\frac{r^2}{N^2} - \frac{\beta^2}{N^3} \right)} \right], \quad (86)$$

which is less computationally demanding to evaluate. Fig. 5 shows examples of the one-point marginal density of the resolvent vector entries for rank-1 NNEMs of the form in Eq. (1), these examples are plotted exactly for $N = 10$ and using the large N approximation for $N = 1000$. These theoretical results are plotted alongside a normalised histogram of results seen in numerical simulation of 1,000,000 samples of rank-1 NNEMs of the form in Eq. (1).

B. One-parameter family of rank-2 NNEMs

In order to find the resolvent and resolvent vector of a general rank-2 NNEM of the form in Eq. (25), one must utilise the Sherman-Morrison formula twice. This leads to the following result

$$\left(\mathbf{1} - \mathbf{x}\mathbf{a}^T - \mathbf{y}\mathbf{b}^T \right)^{-1} = \mathbf{1} + \frac{1 - \mathbf{a}^T \mathbf{x}}{\eta} \mathbf{y}\mathbf{b}^T + \frac{1 - \mathbf{b}^T \mathbf{y}}{\eta} \mathbf{x}\mathbf{a}^T + \frac{\mathbf{a}^T \mathbf{y}}{\eta} \mathbf{x}\mathbf{b}^T + \frac{\mathbf{b}^T \mathbf{x}}{\eta} \mathbf{y}\mathbf{a}^T, \quad (87)$$

where

$$\eta = 1 - \mathbf{b}^T \mathbf{y} - \mathbf{a}^T \mathbf{x} + \mathbf{b}^T \mathbf{y}\mathbf{a}^T \mathbf{x} - \mathbf{b}^T \mathbf{x}\mathbf{a}^T \mathbf{y}. \quad (88)$$

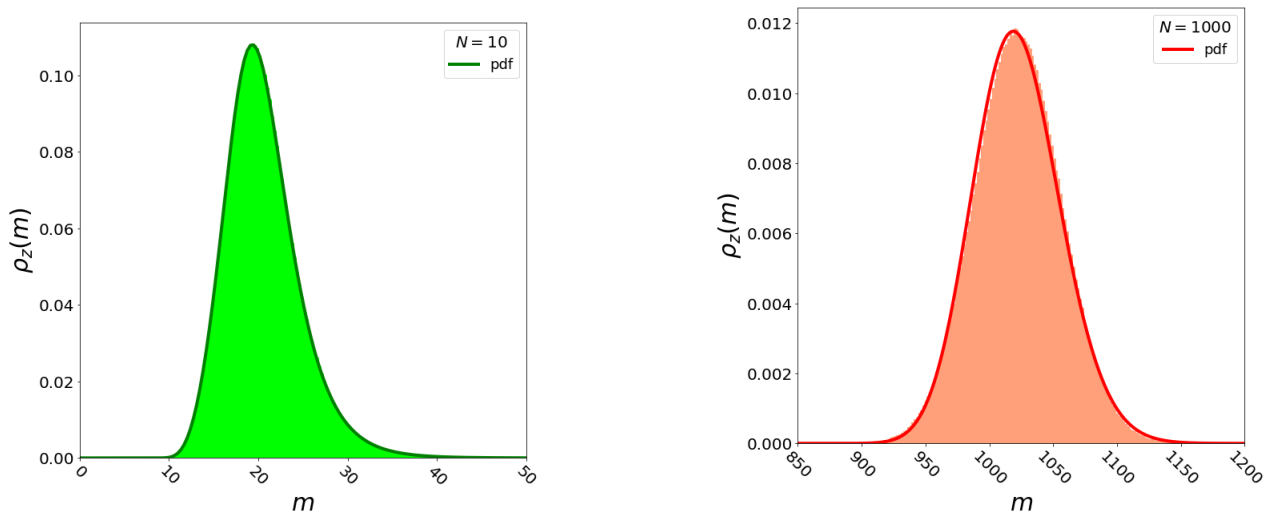


FIG. 5. Probability density functions of the one-point marginal density for the m -vector entries constructed from the resolvent of a rank-1 NNEM of the form in Eq. (1). Left: solid line represents the exact distribution of the one-point marginal density for an NNEM of size $N = 10$, plotted using Eq. (84). Right: solid line represents the large N approximation to the one-point marginal density for an NNEM of size $N = 1000$, plotted using Eq. (86). The numerical simulation of the data obtained for both of these plots was conducted using a fixed set of $\{z_i\}$, generated by removing a random row and column (of the same index) from a row-stochastic matrix of size $N + 1 \times N + 1$. The original row-stochastic matrix had the entries in each row drawn as the entries of a flat Dirichlet random vector. The normalised histogram (shaded region) contains data from 1,000,000 samples of rank-1 NNEMs of the form in Eq. (1) with different sets of $\{a_i\}$.

This can be applied to the one-parameter family of rank-2 matrices in Eq. (26), constructed from the vectors in Eq. (27), such that the entries of the associated resolvent vector read

$$m_j = 1 + \frac{z_j - \epsilon(T(\epsilon) - z_N)}{1 - T(\epsilon) + \epsilon(T(\epsilon) - z_N)}, \quad (89)$$

where one can recall from earlier that

$$T(\epsilon) = \frac{\alpha - Nz_N\epsilon}{\beta - N\epsilon} \quad (90)$$

is the sum of the two non-zero eigenvalues of matrices within this class. Note that if one sets $\epsilon = 0$ and allows the values of a_i to be random then the rank-1 result for the entries of the resolvent vector (in Eq. (81)) is recovered, as one would expect.

C. Comparison of resolvent statistics of low-rank approximations

The main concept behind a low-rank matrix approximation is to measure macroscopic observables of an original matrix and then create an approximate low-rank matrix where some of these macroscopic properties are reproduced [66]. This low-rank matrix is usually much easier to conduct calculations with. Such approximations are useful in the context of finding simple formulas for the mean first passage time of random walkers on complex networks, as these formulas involve only a few macroscopic quantities of the original rank- N matrix and not all the entries [35].

One can now make a comparison between the entries of the resolvent vector obtained using exact inversion of a rank- N matrix and the entries of the resolvent vector generated from matrix approximations. We compare the resolvent vectors of the random rank-1 approximation derived in Eq. (81) and the one-parameter family of rank-2 approximations detailed in Eq. (89). Additionally, it is natural to also compare these results to a pre-existing rank-1 approximation. In the formulation that we consider, the elements in each row are evenly spaced, such that the value of the element (i, j) is given by z_i/N [35]. This will be referred to as the so-called ‘even spacing’ approximation, with

matrix representation

$$T_{ES} = \frac{1}{N} \begin{pmatrix} z_1 & z_1 & \dots & z_1 \\ z_2 & z_2 & \dots & z_2 \\ \vdots & \vdots & \ddots & \vdots \\ z_N & z_N & \dots & z_N \end{pmatrix}, \quad (91)$$

such that the sum of the elements in row i is given by z_i .

In order to accurately conduct this comparison, we consider the following figure of merit

$$\delta = \frac{1}{N} \left\langle \sum_{i=1}^N \left| \left(\mathbf{m}^{(\text{exact})} - \overline{\mathbf{m}^{(\text{approx})}} \right)_i \right| \right\rangle, \quad (92)$$

where $\mathbf{m}^{(\text{exact})}$ is a vector obtained by performing exact inversion with the rank- N matrix, as in Eqs. (79) and (80), and $\mathbf{m}^{(\text{approx})}$ is a vector obtained using a low-rank approximation. The angular brackets indicate an ensemble average over the original rank- N matrices with different sets of $\{z_i\}$ and $\{\zeta_i\}$. The overbar represents a disorder average, this is performed over sets of $\{a_i\}$ for the vectors in Eq. (81) generated using the random rank-1 approximation and over ϵ for the vectors in Eq. (89) generated using the random rank-2 matrix approximation.

The rank- N matrices that were approximated in simulation were drawn in two different ways. Firstly, row sums were drawn from a uniform distribution between $[0, 1]$, then the elements of each row were drawn as flat Dirichlet random variables, constrained to this sum. Column sums were measured once the whole matrix had been drawn. Producing matrices with row sums uniformly distributed between $[0, 1]$ and considering their resolvent vectors gives a general measure of which low-rank approximation provides the most accurate \mathbf{m} -vector. The second method of generating rank- N matrices was to draw a random integer between 1 and N and then remove the column and row with this index from a row-stochastic matrix of size $(N + 1) \times (N + 1)$. This original rank- N row-stochastic matrix was generated with the entries in each independent row being the elements of a flat Dirichlet random vector. Matrices produced by the removal of a row and column from a row-stochastic matrix are reminiscent of the kind used when determining the MFPT [3]. The low-rank approximation that provided the most accurate \mathbf{m} -vector in this case would be the best approximation to use when determining the MFPT. This process was repeated using 100 different rank- N NNEMs of size $N = 500$ and the results are shown in Table III.

Approximation	Measured δ	Approximation	Measured δ
Random rank-1	0.01029	Random rank-1	1.184
Even spaced rank-1 [35]	0.01027	Even spaced rank-1 [35]	0.826
Random rank-2	0.01023	Random rank-2	0.051

TABLE III. Comparison between the entries of the resolvent vector obtained using different low-rank approximations to a rank- N matrix and the true resolvent vector obtained by performing exact inversion with the rank- N matrix. The original rank- N matrix which was approximated was drawn in two different ways. Left: Row sums sampled from a flat distribution between $[0, 1]$. Right: Removing a random row and column of an $(N + 1) \times (N + 1)$ row-stochastic matrix, such that the resulting row sums of the rank- N matrix have mean $1-1/N$. The simulations were carried out using 100 samples of different rank- N matrices of size $N = 500$, each with different sets of $\{z_i\}$ and $\{\zeta_i\}$. The disorder average was conducted using 5000 sets of a_i and ϵ in the rank-1 and rank-2 cases respectively.

From Table III one can see that for a low-rank approximation to a general rank- N matrix all three of the methods provide an approximation to the elements of the \mathbf{m} -vector of comparable quality. However, when considering matrices of the form that arise when studying the MFPT, it is clear that the rank-2 approximation where the row and column sums can be prescribed provides the most accurate approximation to the \mathbf{m} -vector.

Fig. 6 shows a comparison of the accuracy of the 3 approximations mentioned above, when tested in numerical simulation. In this comparison, we show (i) scatter plots of individual entries of the matrix $\mathbf{m}^{(\text{approx})}$ versus the entries of $\mathbf{m}^{(\text{exact})}$ and (ii) scatter plots of the deviation from the exact value of the entry, plotted against the exact value of the entry. This is done for both kinds of original rank- N matrix mentioned above. These Figures corroborate the statement that all three of the methods provide an equally accurate approximation to the entries of the resolvent vector when the matrix has row sums drawn from a flat distribution between $[0, 1]$. Furthermore, they provide further evidence that when considering the MFPT of a random walker, a disorder average over the resolvent vector of the one-parameter family of rank-2 NNEMs described by Eq. (89), provides the most accurate approximation to the MFPT. This is a consequence of the fact that this rank-2 approximation is capable of preserving the highest number of relevant macroscopic characteristics of the original matrix.

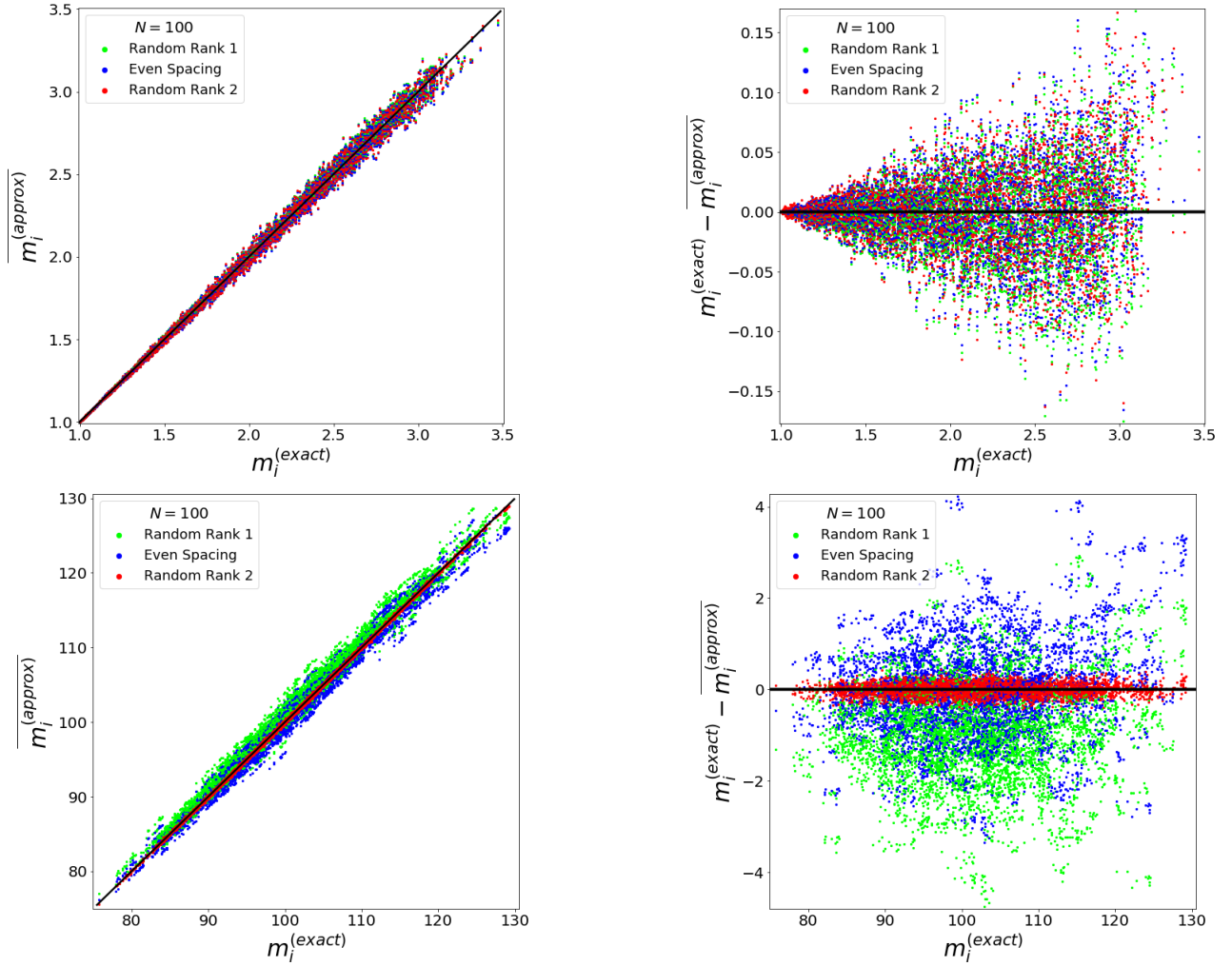


FIG. 6. Scatter plots showing a comparison between entries of the exact resolvent vector obtained by performing inversion with a rank- N matrix and the entries of resolvent vectors generated using low-rank matrix approximations. The 3 considered approximate resolvent vectors were (i) the vector in Eq. (81) derived from the random rank-1 matrix approximation, (ii) the even spacing vector devised by Bartolucci et al. [35] and (iii) the vector described by Eq. (89) derived from the one-parameter family of rank-2 matrix approximations. Top: inverted matrices are drawn with row sums generated from a uniform distribution between $[0, 1]$. Bottom: inverted matrices are substochastic matrices drawn by removing a random row and column, of the same index, from a row-stochastic matrix (as one would do when studying the MFPT). In all plots the solid black line indicates the case where $m_i^{(\text{approx})} = m_i^{(\text{exact})}$. In the more general case where the row sums are drawn uniformly between $[0, 1]$, it can be seen that all 3 methods provide a good and roughly equivalent approximation to the entries of the resolvent vector. However, when considering the MFPT, it is clear that the random rank-2 method provides an approximation with the smallest deviation from the true entries of the resolvent vector. Scatter plots are generated using entries from 500 realisations of different rank- N matrices of size $N = 100$, from which low-rank approximations were generated (for clarity only 10% of the data points are shown).

V. CONCLUSIONS

Matrices with non-negative entries have far-reaching applications in a wide range of fields including complex networks and economics. However, in spite of their deep-rooted presence in many research areas, relatively little is known analytically about their spectra and Extreme Values thereof. The positivity constraint breaks any hope to preserve rotational invariance on the one hand, and to use Gaussian integral representations on the other, thus dramatically reducing the analytical arsenal available to deal with them. The primary aim of this work was to provide some analytic insight into the spectra and statistical properties of such matrices through the use of random low-rank approximations.

We have been able to accurately derive quite a few results pertaining to the eigenvalues, singular values, and

resolvent vectors of two classes of low-rank NNEMs. The models for rank-1 and rank-2 matrices presented in this work provide rare and interesting examples of systems where the full Extreme Value Statistics can be computed analytically for finite matrix size.

Our analysis of rank-1 matrices with prescribed row sums has yielded the full finite N distribution of the Perron-Frobenius eigenvalue and the moments of the only non-zero singular value squared, given by Eqs. (8) and (19) respectively. Additionally, we considered a one-parameter family of rank-2 NNEMs with a further constraint on column sums that led us to understand the interplay between the two non-zero eigenvalues and singular values. The distributions describing the non-zero singular values are particularly interesting due to the presence of discontinuities that can be analytically predicted and verified in simulations.

Furthermore, the resolvent vectors of the rank-1 and rank-2 NNEM approximations to rank- N matrices have been compared to a low-rank (evenly spaced) approximation devised in [35]. This yielded the result that the one-parameter family of rank-2 approximations devised in this work, provides the most accurate approximation to the MFPT of a random walker hopping through the nodes of a complex network. This is by virtue of the fact, that the one-parameter family of rank-2 matrix approximations preserves $2N$ macroscopic quantities of the original matrix, whereas the other approximations only preserve N macroscopic quantities.

The work presented here leads to a few questions worthy of further research. In particular, we have been able to derive a few simple low-rank matrix approximations (preserving macroscopic properties of a full-rank matrix) for which the full Extreme Value Statistics can be derived. This leads one to naturally question whether there are more low-rank approximations that can also be fully analysed? Fruitful extensions could include the preservation of more macroscopic quantities such as: eigenvalues, trace or individual elements. One could also consider methods to optimise an approximation, such that it minimises the difference between true macroscopic quantities and the ones seen in the approximation. Moreover, higher rank approximations can also be considered in an attempt to make more general statements about the statistics of the Perron-Frobenius eigenvalue of rank- k matrices.

ACKNOWLEDGMENTS

Y.V.F. acknowledges financial support from EPSRC Grant EP/V002473/1 ‘‘Random Hessians and Jacobians: theory and applications’’. M.J.C. is supported by a studentship from the Faculty of Natural and Mathematical Sciences at King’s College London.

Appendix A: Proof of the identity used to derive properties of rank-1 NNEMs

In Sec. II and Sec. IV we made use of the following identity,

$$\sum_{k=1}^N \frac{z_k^m}{\prod_{l \neq k} (z_k - z_l)} = \begin{cases} 0 & [m = 0, 1, 2, \dots, N - 2] \\ 1 & [m = N - 1] \end{cases}. \quad (\text{A1})$$

This was highly useful for deriving various statistical properties of rank-1 NNEMs of the form in Eq. (1). These properties include the distribution of the Perron-Frobenius eigenvalue and the one-point marginal density of the entries of the associated resolvent vector. In order to provide the reader with a proof, it is convenient to consider the following identity

$$\frac{1}{\prod_{i=1}^N (z_i - x)} = (-1)^N \sum_{k=1}^N \frac{1}{\prod_{l \neq k} (z_k - z_l)} \frac{1}{x - z_k}, \quad (\text{A2})$$

which can be easily checked by induction on partial fractions. Combining this with the expansion at $x \rightarrow \infty$:

$$\frac{1}{x - z_k} = \frac{1}{x} + \frac{z_k}{x^2} + \frac{z_k^2}{x^3} + \dots, \quad (\text{A3})$$

we get upon substituting in Eq (A2) and rearranging in inverse powers of x the following equality:

$$\frac{1}{\prod_{i=1}^N (z_i - x)} = (-1)^N \left[\frac{1}{x} \sum_{k=1}^N \frac{1}{\prod_{l \neq k} (z_k - z_l)} + \frac{1}{x^2} \sum_{k=1}^N \frac{z_k}{\prod_{l \neq k} (z_k - z_l)} + \dots + \frac{1}{x^N} \sum_{k=1}^N \frac{z_k^{N-1}}{\prod_{l \neq k} (z_k - z_l)} + \dots \right]. \quad (\text{A4})$$

As obviously the LHS for large x has the leading behaviour of the form

$$\frac{1}{\prod_{i=1}^N (z_i - x)} \sim \frac{(-1)^N}{x^N}, \quad (\text{A5})$$

it should match the corresponding asymptotics of the RHS. Hence, all the coefficients in front of $1/x^k$ with $k = 1, \dots, N-1$ must vanish, and the coefficient in front of $1/x^N$ must yield unity, producing exactly the required identities in Eq. (A1).

Appendix B: Derivation of k -th moment of the squared singular value σ^2

In order to determine the moments of the non-zero squared singular value of a rank-1 NNEM of the form in Eq. (1), given by

$$\sigma^2 = r^2 \left(\sum_{i=1}^N a_i^2 \right), \quad (\text{B1})$$

one must perform an average over possible sets of $\{a_i\}$. Using the multinomial theorem

$$\langle (\sigma^2)^k \rangle = C_N r^{2k} \int_0^\infty da_1 \int_0^\infty da_2 \cdots \int_0^\infty da_N (a_1^2 + a_2^2 + \dots + a_N^2)^k \delta \left(\sum_{i=1}^N a_i - 1 \right) \quad (\text{B2})$$

$$= C_N r^{2k} \sum_{k_1+k_2+\dots+k_N=k} \binom{k}{k_1, k_2, \dots, k_N} I(\mathbf{k}), \quad (\text{B3})$$

where

$$I(\mathbf{k}) = \int_0^\infty da_1 \int_0^\infty da_2 \cdots \int_0^\infty da_N \prod_{i=1}^N a_i^{2k_i} \delta \left(\sum_{i=1}^N a_i - 1 \right) \quad (\text{B4})$$

and

$$\binom{k}{k_1, k_2, \dots, k_N} = \frac{k!}{k_1! k_2! \cdots k_N!} \quad (\text{B5})$$

is the multinomial coefficient.

To compute $I(\mathbf{k})$, we first introduce the auxiliary quantity

$$I(\mathbf{k}, t) = \int_0^\infty da_1 \int_0^\infty da_2 \cdots \int_0^\infty da_N \prod_{i=1}^N a_i^{2k_i} \delta \left(\sum_{i=1}^N a_i - t \right) \quad (\text{B6})$$

and then compute its Laplace transform w.r.t. t

$$\hat{I}(\mathbf{k}, s) = \int_0^\infty dt e^{-st} I(\mathbf{k}, t) = \int_0^\infty da_1 \int_0^\infty da_2 \cdots \int_0^\infty da_N \prod_{i=1}^N a_i^{2k_i} e^{-s \sum_i a_i} = \prod_{i=1}^N \frac{(2k_i)!}{s^{2k_i+1}}. \quad (\text{B7})$$

Inverting the Laplace transform

$$I(\mathbf{k}, t) = \frac{t^{2k+N-1}}{\Gamma(2k+N)} \prod_{i=1}^N (2k_i)!, \quad (\text{B8})$$

where $k = \sum_i k_i$. Setting $t = 1$, we eventually get after simplifications

$$\langle (\sigma^2)^k \rangle = (N-1)! \frac{r^{2k} k!}{(2k+N-1)!} \varphi(k, N), \quad (\text{B9})$$

where

$$\varphi(k, N) = \sum_{k_1+k_2+\dots+k_N=k} \prod_{i=1}^N \frac{(2k_i)!}{k_i!}. \quad (\text{B10})$$

The sum over partitions of k is however exponentially hard to evaluate even for moderate N . A friendlier expression can be found using the Faá di Bruno formula. We can write

$$\begin{aligned} \varphi(k, N) &= \sum_{k_1+\dots+k_N=k} \prod_i \frac{(2k_i)!}{k_i!} = \sum_{k_1=0}^k \dots \sum_{k_N=0}^k \prod_i \frac{(2k_i)!}{k_i!} \delta_{\sum_i k_i, k} \\ &= \frac{1}{2\pi i} \oint_{|z|=1} dz \sum_{k_1=0}^k \dots \sum_{k_N=0}^k \prod_i \frac{(2k_i)!}{k_i!} z^{\sum_i k_i - k - 1} = \frac{1}{2\pi i} \oint_{|z|=1} dz \frac{1}{z^{k+1}} \left[\sum_{m=0}^k \frac{(2m)!}{m!} z^m \right]^N, \end{aligned} \quad (\text{B11})$$

where we have used the integral representation of the Kronecker delta in the second line. Using the residue theorem

$$\varphi(k, N) = \frac{1}{k!} \lim_{z \rightarrow 0} \frac{d^k}{dz^k} \left[\sum_{m=0}^k \frac{(2m)!}{m!} z^m \right]^N. \quad (\text{B12})$$

For the case where $k = 0$, $\varphi(0, N) = 1$, hence the $\langle (\sigma^2)^0 \rangle = 1$ as expected. We can now use the Faá di Bruno formula for the k -th derivative of the composition of two functions

$$\frac{d^k}{dz^k} \phi(g(z)) = \sum_{\ell=1}^k \phi^{(\ell)}(g(z)) B_{k,\ell}(g'(z), g''(z), \dots, g^{(k-\ell+1)}(z)), \quad (\text{B13})$$

where $\phi^{(\ell)}(x)$ is the ℓ -th derivative of ϕ , k is a positive integer and $B_{k,\ell}$ are Bell polynomials. In Eq. (B12) we have

$$\phi(x) = x^N \quad \text{and} \quad g(z) = \sum_{m=0}^k f(m) z^m, \quad (\text{B14})$$

with $f(m) = (2m)!/m!$ and derivatives

$$\left. \phi^{(\ell)}(g(z)) \right|_{z=0} = \Theta[N - \ell] \frac{N!}{(N - \ell)!} \left[\sum_{m=0}^k f(m) z^m \right]^{N - \ell} \Big|_{z=0} = \Theta[N - \ell] \frac{N!}{(N - \ell)!}, \quad (\text{B15})$$

since $f(0) = 1$. Additionally, it is easy to see that the ℓ -th derivative of g is given by

$$g^{(\ell)}(z = 0) = \ell! f(\ell) \Theta[l - k]. \quad (\text{B16})$$

Using these results we can re-express $\varphi(k, N)$ as

$$\varphi(k, N) = \begin{cases} 1 & [k = 0] \\ \frac{1}{k!} \sum_{\ell=1}^{\min(N,k)} \frac{N!}{(N-\ell)!} B_{k,\ell}(f(1), 2!f(2), \dots, (k-\ell+1)!f(k-\ell+1)) & [k \geq 1] \end{cases}, \quad (\text{B17})$$

therefore the expression for the k -th moment becomes

$$\langle (\sigma^2)^k \rangle = \begin{cases} 1 & [k = 0] \\ r^{2k} \frac{(N-1)!}{(2k+N-1)!} \sum_{\ell=1}^{\min(N,k)} \frac{N!}{(N-\ell)!} B_{k,\ell}(f(1), 2!f(2), \dots, (k-\ell+1)!f(k-\ell+1)) & [k \geq 1] \end{cases}. \quad (\text{B18})$$

Appendix C: Exact pdfs of the non-zero singular value squared of rank-1 NNEMs

The formula for the distribution of the non-zero singular value squared of an $N \times N$ rank-1 NNEM of the form in Eq. (1), is related to

$$\mathcal{P}_{\mathbf{z},N}(\sigma^2, t) = C_N \int_0^\infty da_1 \int_0^\infty da_2 \dots \int_0^\infty da_N \delta\left(\sigma^2 - r^2 \sum_{i=1}^N a_i^2\right) \delta\left(\sum_{i=1}^N a_i - t\right), \quad (\text{C1})$$

where $r^2 = \sum_i z_i^2$ and t is an auxiliary variable such that $\sum_i a_i = t$. This can be explicitly evaluated for $N = 1$ to give

$$\mathcal{P}_{\mathbf{z},1}(\sigma^2, t) = \delta(\sigma^2 - r^2 t^2), \quad (\text{C2})$$

which can be used in the iterative formula

$$\mathcal{P}_{\mathbf{z},N}(\sigma^2, t) \propto \int da_N \mathcal{P}_{\mathbf{z},N-1}(\sigma^2 - r^2 a_N^2, t - a_N), \quad (\text{C3})$$

for the pdf of the non-zero singular value squared of a general rank-1 NNEM with prescribed row sums. This equation can, in principle, be evaluated explicitly to give the pdf for any N . Starting from $N = 1$, one can explicitly derive the pdfs for $N = 2$ and $N = 3$, given by

$$\mathcal{P}_{\mathbf{z},2}(\sigma^2) = \begin{cases} \frac{1}{r} \frac{1}{\sqrt{2\sigma^2 - r^2}} & \left[\frac{r^2}{2} \leq \sigma^2 \leq r^2\right] \\ 0 & [\text{elsewhere}] \end{cases} \quad (\text{C4})$$

and

$$\mathcal{P}_{\mathbf{z},3}(\sigma^2) = \frac{2}{\sqrt{3}r^2} \begin{cases} \pi & \left[\frac{r^2}{3} \leq \sigma^2 \leq \frac{r^2}{2}\right] \\ \left[\frac{\pi}{2} - \arcsin\left(\frac{3r}{\sqrt{6\sigma^2 - 2r^2}} \left(\frac{1}{6} + \frac{1}{2}\sqrt{\frac{2\sigma^2}{r^2} - 1}\right)\right) + \right. \\ \left. \arcsin\left(\frac{3r}{\sqrt{6\sigma^2 - 2r^2}} \left(\frac{1}{6} - \frac{1}{2}\sqrt{\frac{2\sigma^2}{r^2} - 1}\right)\right) + \arcsin\left(\frac{r}{\sqrt{6\sigma^2 - 2r^2}}\right) \right] & \left[\frac{r^2}{2} \leq \sigma^2 \leq r^2\right] \\ 0 & [\text{elsewhere}] \end{cases} \quad (\text{C5})$$

respectively. Interestingly, the distribution of the non-zero squared singular value of a 3×3 NNEM is uniform between $r^2/3$ and $r^2/2$. This result is similar to a result obtained earlier by Weissman and Ben-Israel [59], where it was shown that the sum of the squares of two uniform random variables drawn between $[0, 1]$ has a uniform distribution between $[0, 1]$ and then decreasing density between $[1, 2]$. Fig. 7 shows a comparison between the above theoretical pdfs and normalised histograms of values obtained from numerical simulation of rank-1 NNEMs. One must be extremely careful when evaluating these integrals as the limits on a_N are non-trivial. The $N - 1$ pdf, $\mathcal{P}_{\mathbf{z},N-1}(\sigma^2)$, consists of a spline of $N - 2$ non-zero regions. Non-zero region n is valid for values of σ^2 between $r^2 t^2 / (N - n + 1)$ and $r^2 t^2 / (N - n)$, thus each non-zero region must be integrated over values of a_N that satisfy both:

$$\frac{r^2(t - a_N)^2}{(N - n + 1)} \leq \sigma^2 - r^2 a_N^2 \leq \frac{r^2(t - a_N)^2}{(N - n)} \quad \text{and} \quad 0 \leq a_N \leq t. \quad (\text{C6})$$

Numerical integration can then be utilised to accurately predict the pdf of the non-zero singular value squared for higher values of N . Note that the distribution of the sum of squares of N Dirichlet random variables can be obtained from the above equations by setting $r = 1$.

Appendix D: Exact pdfs of individual eigenvalues and spectral gap in rank-2 approximation

We now consider the derivation of the probability distribution function of the spectral gap given by

$$G(\epsilon) = \lambda_1(\epsilon) - \lambda_2(\epsilon) = \sqrt{T(\epsilon)^2 - 4D(\epsilon)}. \quad (\text{D1})$$

For ease of computation, the choice can be made to calculate the pdf in terms of

$$G^2(\epsilon) = \frac{(\alpha - Nz_N \epsilon)^2 - 4\epsilon(\alpha - z_N \beta)(\beta - N\epsilon)}{(\beta - N\epsilon)^2}, \quad (\text{D2})$$

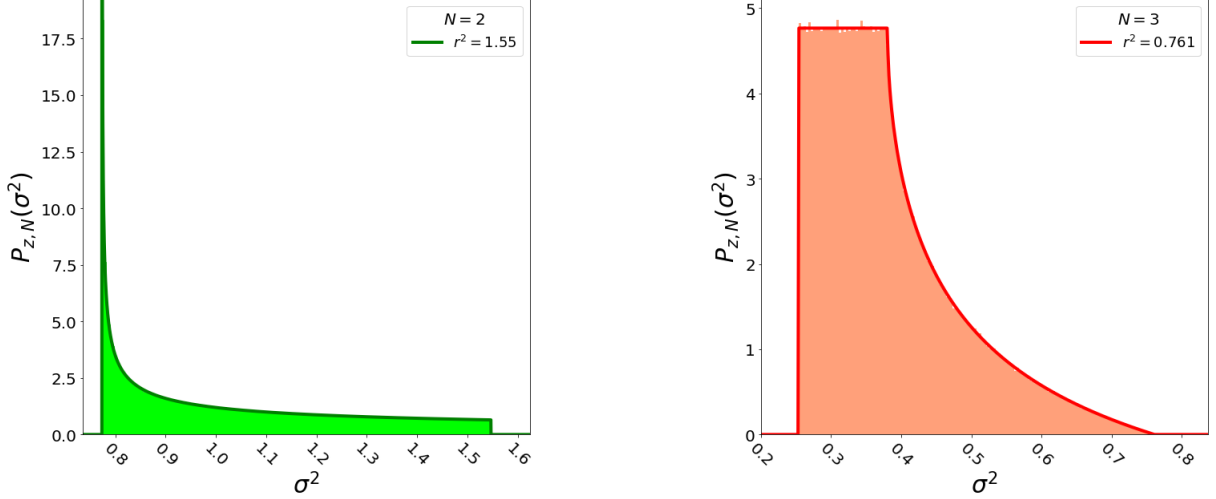


FIG. 7. Probability distribution functions of the non-zero singular value squared of a rank-1 NNEM of the form in Eq. (1) with uniformly distributed sets of $\{z_i\}$ drawn between $[0, 1]$. In both plots the solid line represent a different pdf. Left: Exact pdf from Eq. (C4) for an $N = 2$ matrix. Right: Exact pdf from Eq. (C5) for an $N = 3$ matrix. Each plot contains a normalised histogram (shaded region) of observed singular values from simulation of 1,000,000 rank-1 matrices of the form in Eq. (1) with different sets of $\{a_i\}$.

first and then employ a change of probabilistic variables so as to obtain the pdf $P(G)$. The first derivative of $G^2(\epsilon)$ can be seen to be proportional to $\alpha - z_N\beta$. Thus, in a similar way to when studying the distribution of T and D , the sign of $\alpha - z_N\beta$ effects the overall shape of the pdf. The function $G^2(\epsilon)$ has a global minimum at the coordinates

$$(\epsilon_s, G_{\min}^2) = \left(\frac{\beta}{N} + \frac{\alpha - z_N\beta}{Nz_N - 2\beta}, \frac{4(N\alpha - \beta^2)}{N^2} \right), \quad (\text{D3})$$

and so the pdf of G^2 must be zero below the critical value G_{\min}^2 . The pdf as a function of G^2 is derived starting from

$$P(G^2) = C_\epsilon \int_{\epsilon_{\min}}^{\epsilon_{\max}} d\epsilon \delta \left(G^2 - \frac{(\alpha - Nz_N\epsilon)^2 - 4\epsilon(\alpha - z_N\beta)(\beta - N\epsilon)}{(\beta - N\epsilon)^2} \right), \quad (\text{D4})$$

and to evaluate this integral, one must first locate the roots of the function inside the δ in terms of ϵ . For a given value of G^2 , there are two possible roots that can, but are not guaranteed, to be within the support of ϵ . The structure of the pdf then follows from determining which solutions are within the support of ϵ for a given value of G^2 . Then, by carrying out the transformation of $G^2 \rightarrow G$, one finds that the pdf of the spectral gap is given by

$$P(G) = C_\epsilon \begin{cases} 0 & [G \leq G_{\min}] \\ \mathcal{P}_+(G) + \mathcal{P}_-(G) & [G_{\min} < G \leq G'] \\ \Theta[G(\epsilon_{\max}) - G(\epsilon_{\min})] \mathcal{P}_-(G) + \Theta[G(\epsilon_{\min}) - G(\epsilon_{\max})] \mathcal{P}_+(G) & [G' < G \leq G_{\max}] \\ 0 & [G > G_{\max}] \end{cases}, \quad (\text{D5})$$

where

$$\mathcal{P}_\pm(G) = \frac{G}{\gamma(G)} \frac{[(2\beta - Nz_N)(\alpha - z_N\beta) \pm \gamma(G)]^2}{(G^2N - Nz_N^2 - 4\alpha + 4z_N\beta)^2}, \quad (\text{D6})$$

and

$$\gamma(G) = \sqrt{(\alpha - z_N\beta)^2(G^2N^2 - 4N\alpha + 4\beta^2)}. \quad (\text{D7})$$

The important values of G for which the nature of the spline pdf changes are given by

$$G_{\min} = \begin{cases} G(\epsilon_s) & [\epsilon_{\min} < \epsilon_s < \epsilon_{\max}] \\ \min[G(\epsilon_{\min}), G(\epsilon_{\max})] & [\text{otherwise}] \end{cases} \quad (\text{D8})$$

$$G' = \min[G(\epsilon_{\min}), G(\epsilon_{\max})] \quad (\text{D9})$$

$$G_{\max} = \max[G(\epsilon_{\min}), G(\epsilon_{\max})]. \quad (\text{D10})$$

Note that this distribution has a potential discontinuity at the point $G = G'$, which is seen if ϵ_s is within the support of allowed values for ϵ . From considering Eq. (D3) and the conditions for non-negativity of the entries outlined in Sec. III, one can see that if $\epsilon_s > \beta/N$, then ϵ_s never belongs to the range of allowed ϵ . Thus, the sign of the product $(\alpha - z_N\beta)(Nz_N - 2\beta)$ controls if the discontinuity can be seen or not. This potential discontinuity is similar to what is seen when studying the distributions of τ and Δ , however it is observed much less frequently in numerical simulation of rank-2 matrices of the form in Eq. (26).

Finally, one can analyse the pdfs of the individual eigenvalues. In order to learn more about these distributions one should utilise the joint distribution

$$P(T, D) = C_\epsilon \int d\epsilon \delta\left(T - \frac{\alpha - Nz_N\epsilon}{\beta - N\epsilon}\right) \delta\left(D - \frac{\epsilon(\alpha - z_N\beta)}{\beta - N\epsilon}\right), \quad (\text{D11})$$

such that

$$P(\lambda_{1,2}) = C_\epsilon \int d\epsilon dT dD P(T, D) \delta\left(\lambda_{1,2} - \frac{T}{2} \mp \frac{1}{2} \sqrt{T^2 - 4D}\right). \quad (\text{D12})$$

In contrast to the distributions of the spectral gap and the sum and product of the singular values, the functions $\lambda_{1,2}(\epsilon)$ are always one-to-one. Thus, the pdfs have no discontinuities within the support of allowed eigenvalues. It is also important to note that the first derivative of the functions $\lambda_{1,2}(\epsilon)$ are once again proportional to the value of $\alpha - z_N\beta$, further reinforcing the importance of the sign of this matrix specific constant. This manifests itself in the definition of the support of the eigenvalues as

$$\lambda_{1,2}^{\min} = \begin{cases} \lambda_{1,2}(\epsilon_{\min}) \\ \lambda_{1,2}(\epsilon_{\max}) \end{cases} \quad \text{and} \quad \lambda_{1,2}^{\max} = \begin{cases} \lambda_{1,2}(\epsilon_{\max}) & [\alpha > z_N\beta] \\ \lambda_{1,2}(\epsilon_{\min}) & [\alpha < z_N\beta] \end{cases}. \quad (\text{D13})$$

Following the standard procedure of integrating a complicated δ function, one finds that the probability distributions of the individual eigenvalues are given by

$$P(\lambda_{1,2}) = C_\epsilon \begin{cases} \frac{2\Gamma_{1,2}}{(\alpha - z_N\beta + Nz_N\lambda_{1,2} - N\lambda_{1,2}^2)^2} \left| \frac{(\alpha - z_N\beta)(\beta - N\lambda_{1,2})^3}{2\beta^2 - N[\alpha - N\lambda_{1,2}(\lambda_{1,2} \pm \Gamma_{1,2}) + \beta(2\lambda_{1,2} \pm \Gamma_{1,2})]} \right| & [\lambda_{1,2}^{\min} \leq \lambda_{1,2} \leq \lambda_{1,2}^{\max}] \\ 0 & [\text{otherwise}] \end{cases}, \quad (\text{D14})$$

where the positive (negative) solution is for $P(\lambda_{1(2)})$ and

$$\Gamma_{1,2} = \sqrt{\left(\frac{\alpha + \lambda_{1,2}(N\lambda_{1,2} - 2\beta)}{\beta - N\lambda_{1,2}}\right)^2}. \quad (\text{D15})$$

In Fig. 8, we show theoretical distributions of the individual eigenvalues and the spectral gap generated from Eqs. (D14) and (D5) respectively. These are plotted alongside a normalised histogram of 1,000,000 samples of eigenvalues obtained in numerical simulation of rank-2 matrices of the form in Eq. (26). Once again, it is apparent that the shape of the distribution is dependent on the sign of $\alpha - z_N\beta$.

-
- [1] J. G. Kemeny and J. L. Snell. *Finite Markov Chains*. Springer, New York (1976).
[2] E. Seneta. *Non-negative matrices and Markov chains*, Springer, New York (1981).
[3] N. Masuda, M. A. Porter and R. Lambiotte. Random walks and diffusion on networks. *Physics Reports* **716-717**, 1-5 (2017). <https://doi.org/10.1016/j.physrep.2017.07.007>.
[4] W. J. Hendricks. The Stationary Distribution of an Interesting Markov Chain. *Journal of Applied Probability* **9** (1), 231-233 (1972).
[5] C. R. Johnson. Row Stochastic Matrices Similar to Doubly Stochastic Matrices. *Linear and Multilinear Algebra* **10** (2), 113-130 (1981). <https://doi.org/10.1080/03081088108817402>.
[6] R. D. Sinkhorn and P. J. Knopp. Concerning nonnegative matrices and doubly stochastic matrices. *Pacific Journal of Mathematics* **21** (2), 343-348 (1967). DOI: 10.2140/pjm.1967.21.343.
[7] S. Chatterjee, P. Diaconis and A. Sly. Properties of Uniform Doubly Stochastic Matrices. arXiv:1010.6136 [math.PR] (2010).
[8] V. Cappellini, H-J. Sommers, W. Bruzda and K. Życzkowski. Random bistochastic matrices. *Journal of Physics A: Mathematical and Theoretical* **42** (36), 365209 (2009).

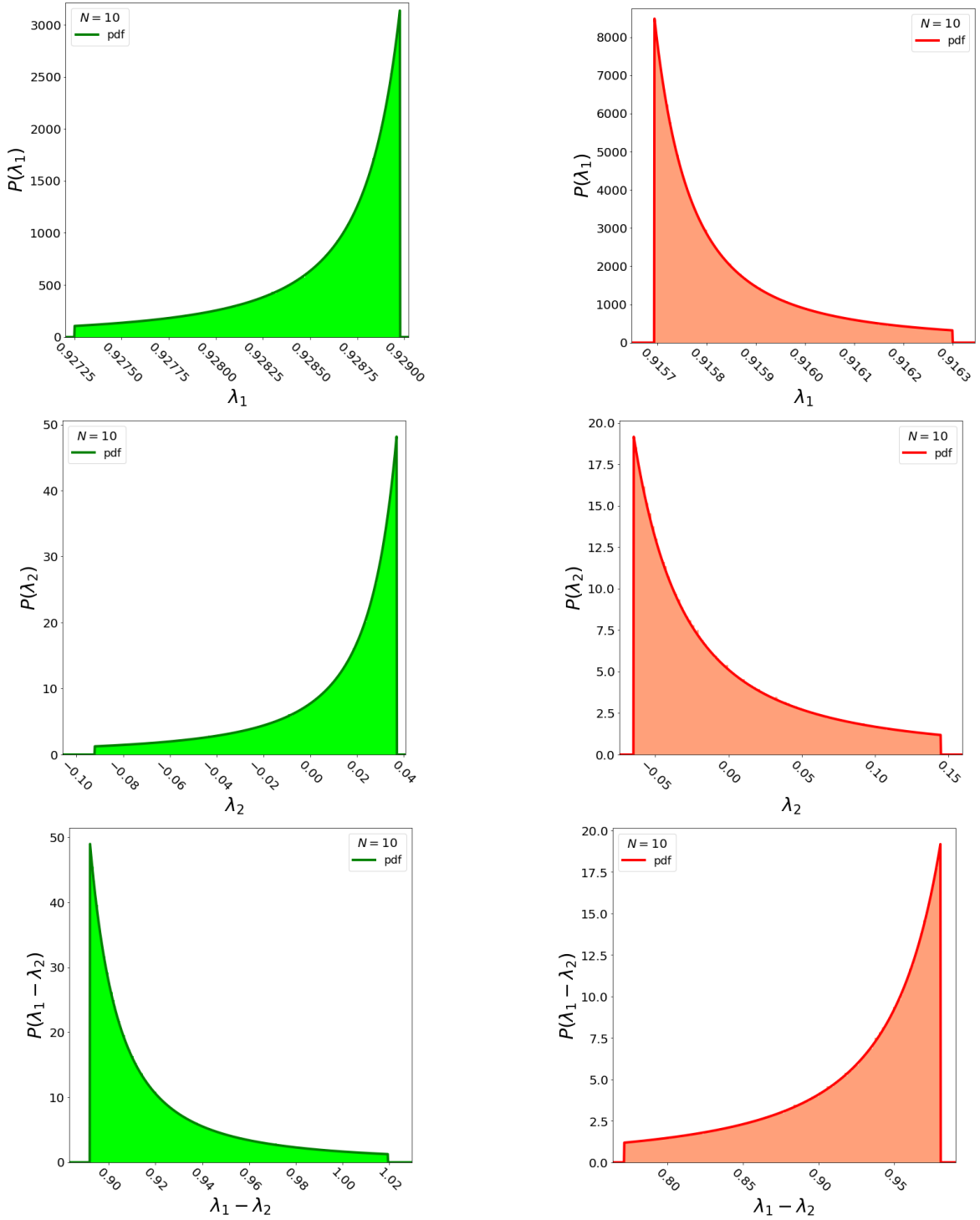


FIG. 8. Probability distributions of the individual eigenvalues and spectral gap of non-zero eigenvalues of matrices within the one-parameter family of rank-2 NNEMs described in Eq. (26). The green plots on the left-hand side indicate matrices with $\alpha < z_N \beta$ whereas the red plots on the right-hand side indicate matrices with $\alpha > z_N \beta$. Each plot contains a theoretical pdf (solid line), generated according to Eqs. (D14) and (D5) for the individual eigenvalues and the spectral gap respectively. The plots also show a normalised histogram (shaded region) of 1,000,000 samples of eigenvalues obtained from numerical simulation of $N = 10$ matrices. Note how the plots appear to mirror each other and how, for these sets of $\{z_i\}$ and $\{\zeta_i\}$, the distributions of the spectral gap possess no discontinuities of the kind seen earlier. The fixed row and column sums are generated by observing the row and column sums of a substochastic matrix created by removing a random row and column, of the same index, from an original row-stochastic matrix of size $N + 1 \times N + 1$. The entries of each independent row of the original stochastic matrix were drawn as the elements of a flat Dirichlet random vector.

- [9] W. Leontief. Environmental Repercussions and the Economic Structure: An Input-Output Approach. *The Review of Economics and Statistics* **52** (3), 262-271 (1970).
- [10] J. McNerney, C. Savoie, F. Caravelli, V. M. Carvalho and J. Doyne Farmer. How production networks amplify economic growth. *Proceedings of the National Academy of Sciences* **119** (1), e2106031118 (2021).
- [11] R. E. Miller and U. Temurshoev. Output Upstreamness and Input Downstreamness of Industries/Countries in World Production. *International Regional Science Review* **40** (5), 443-475 (2017). DOI: 10.1177/0160017615608095.
- [12] P. Antrás, D. Chor, T. Fally and R. Hillberry. Measuring the Upstreamness of Production and Trade Flows. *American Economic Review* **102** (3), 412-416 (2012).
- [13] R. E. Miller and P. D. Blair. *Input-Output Analysis: Foundations and Extensions*, Second Edition, Cambridge University Press, Cambridge (2009).
- [14] H. E. Bray. Rates of Exchange. *The American Mathematical Monthly* **29** (10), 365-371 (1922). doi: 10.1080/00029890.1922.11986177.
- [15] I. G. Ivanov. On a Class of Nonnegative Matrices in Mathematical Economics Models. *Comptes rendus de l'Académie bulgare des Sciences* **54** (12), 12-19 (2001).
- [16] L. Zeng. Effects of changes in outputs and in prices on the economic system: an input-output analysis using the spectral theory of nonnegative matrices. *Economic Theory* **34**, 441-471 (2008), doi:10.1007/s00199-006-0197-0.
- [17] G. Debreu and I. N. Herstein. Nonnegative Square Matrices. *The Econometric Society: Econometrica* **21** (4), 597-607 (1953).
- [18] S. Bartolucci, F. Caccioli, F. Caravelli and P. Vivo. Inversion-free Leontief inverse: statistical regularities in input-output analysis from partial information. Preprint arXiv:2009.06350 (2020).
- [19] T. E. S. Raghavan. On Positive Game Matrices and Their Extensions. *Journal of London Mathematical Society* **40** (1), 467-477 (1965).
- [20] R. L. Weil Jr. Game theory and eigensystems. *SIAM Review* **10** (3), 360-367 (1968).
- [21] F. Sing. Some Results on Matrices with Prescribed Diagonal Elements and Singular Values. *Canadian Mathematical Bulletin* **19** (1), 89-92 (1976). doi:10.4153/CMB-1976-012-5.
- [22] R. B. Bapat and T. E. S. Raghavan. *Nonnegative Matrices and Applications*. Encyclopedia of Mathematics and its Applications, Cambridge University Press, Cambridge, (1997). doi:10.1017/CBO9780511529979.
- [23] O. Perron. Grundlagen für eine Theorie des Jacobischen Kettenbruchalgorithmus. *Mathematische Annalen* **64** (1), 1-76 (1907).
- [24] O. Perron. Zur Theorie der Matrizen. *Mathematische Annalen* **64** (2), 248-263 (1907).
- [25] G. Frobenius. Über Matrizen aus positiven Elementen. *Sitzungsberichte der Königlich Preussischen Akademie der Wissenschaften*, 471-476 (1908).
- [26] G. Frobenius. Über Matrizen aus positiven Elementen II. *Sitzungsberichte der Königlich Preussischen Akademie der Wissenschaften*, 514-518 (1909).
- [27] G. Frobenius. Ueber Matrizen aus nicht negativen Elementen. *Sitzungsberichte der Königlich Preussischen Akademie der Wissenschaften*, 456-477 (1912).
- [28] S. U. Pillai, T. Suel and S. Cha. The Perron-Frobenius Theorem: Some of its applications. *IEEE Signal Processing Magazine*, 22 (2), 62-75 (2005).
- [29] J. Ginibre. Statistical Ensembles of Complex, Quaternion, and Real Matrices. *Journal of Mathematical Physics* **6** (3), 440-449 (1965).
- [30] V. L. Girko. Circular Law. *Theory of Probability and its Applications* **29** (4), 694-706 (1985).
- [31] F. Benaych-Georges and R. R. Nadakuditi. The eigenvalues and eigenvectors of finite, low rank perturbations of large random matrices. *Advances in Mathematics* **227** (1), 494-521 (2011). <https://doi.org/10.1016/j.aim.2011.02.007>.
- [32] T. Tao. Outliers in the spectrum of iid matrices with bounded rank perturbations. *Probability Theory and Related Fields* **155**, 231-263 (2013).
- [33] C. Bordenave, P. Caputo and D. Chafaï. Circular law theorem for random Markov matrices. *Probability Theory and Related Fields* **152** (3), 751-779 (2012).
- [34] F. Mosam, D. Vidaurre and E. De Giulì. Breakdown of random matrix universality in Markov models. *Phys. Rev. E* **104** (2), 024305 (2021). 10.1103/PhysRevE.104.024305.
- [35] S. Bartolucci, F. Caccioli, F. Caravelli and P. Vivo. "Spectrally gapped" random walks on networks: a Mean First Passage Time formula. *SciPost Phys* **11** (5), 88 (2021). 10.21468/SciPostPhys.11.5.088.
- [36] C. A. Tracy and H. Widom. Level-spacing distributions and the Airy kernel. *Communications in Mathematical Physics* **159** (1), 151-174 (1994).
- [37] M. Jerrum, A. Sinclair and E. Vigoda. A Polynomial-Time Approximation Algorithm for the Permanent of a Matrix with Nonnegative Entries. *Journal of the ACM* **51** (4), 671-697 (2004). <https://doi.org/10.1145/1008731.1008738>.
- [38] S. Dhara, D. Mukherjee and K. Ramanan. On r-to-p norms of random matrices with nonnegative entries: Asymptotic normality and l_∞ -bounds for the maximizer. arXiv:2005.14056 [math.PR] (2020).
- [39] G. Högnäs and A. Mukherjee. Products of I.I.D. Random Nonnegative Matrices: Their Skeletons and Convergence in Distribution. *The Indian Journal of Statistics (2003-2007)* **67** (4), 615-633 (2005).
- [40] H. Hennion. Limit Theorems for Products of Positive Random Matrices. *The Annals of Probability* **25** (4), 1545-1587 (1997).
- [41] J. Mierczyński. Averaging in random systems of nonnegative matrices. *Dynamical Systems, Differential Equations and Applications AIMS Proceedings* **2015**, 835-840 (2015). doi:10.3934/proc.2015.0835.
- [42] J. G. Restrepo, E. Ott and B. R. Hunt. Approximating the largest eigenvalue of network adjacency matrices. *Physical*

- Review E **76** (5), 056119 (2007). doi:10.1103/PhysRevE.76.056119.
- [43] M. Ng, L. Qi, and G. Zhou. Finding the Largest Eigenvalue of a Nonnegative Tensor. *SIAM Journal on Matrix Analysis and Applications* **31** (3), 1090–1099 (2009).
- [44] V. Nikiforov. Some Inequalities for the Largest Eigenvalue of a Graph. *Combinatorics, Probability and Computing* **11** (2), 179–189 (2002). doi:10.1017/S0963548301004928.
- [45] V. A. R. Susca, P. Vivo and R. Kühn. Cavity and replica methods for the spectral density of sparse symmetric random matrices. *SciPost Physics Lecture Notes* **33** (2021).
- [46] J. E. Cohen and U. G. Rothblum. Nonnegative ranks, decompositions, and factorizations of nonnegative matrices. *Linear Algebra and its Applications* **190** 149–168 (1993).
- [47] T. Squartini and D. Garlaschelli. *Maximum-Entropy Networks: Pattern Detection, Network Reconstruction and Graph Combinatorics*. Springer, New York (2017).
- [48] T. Squartini, G. Caldarelli, G. Cimini, A. Gabrielli and D. Garlaschelli. Reconstruction methods for networks: The case of economic and financial systems. *Physics Reports* **757**, 1–47 (2018).
- [49] G. Cimini, T. Squartini, D. Garlaschelli and A. Gabrielli. Systemic Risk Analysis on Reconstructed Economic and Financial Networks. *Scientific Reports* **5**, 15758 (2015).
- [50] L. Zeng, Y. He, M. Povolotskyi, X. Liu, G. Klimeck and T. Kubis. Low rank approximation method for efficient Green’s function calculation of dissipative quantum transport. *Journal of Applied Physics* **113**, 213707 (2013).
- [51] R. Yokota, H. Ibeid and D. Keyes. Fast multipole method as a matrix-free hierarchical low-rank approximation. In *International Workshop on Eigenvalue Problems: Algorithms, Software and Applications in Petascale Computing*. Springer, 267–286 (2015).
- [52] L. Lestandi. Numerical Study of Low Rank Approximation Methods for Mechanics Data and Its Analysis. *Journal of Scientific Computing* **87** (14), 1–43 (2021). <https://doi.org/10.1007/s10915-021-01421-2>.
- [53] G. Livan, M. Novaes and P. Vivo. *Introduction to Random Matrices: Theory and Practice*. Springer: SpringerBriefs in Mathematical Physics **26** (2018).
- [54] S. Bartolucci, F. Caravelli, F. Caccioli and P. Vivo. Emerging locality of network influence. PrePrint arXiv:2009.06307 (2021).
- [55] I. Neri and F. L. Metz. Eigenvalue Outliers of Non-Hermitian Random Matrices with a Local Tree Structure. *Physical Review Letters* **117** (22), 224101 (2016).
- [56] I.G. Macdonald. *Symmetric Functions and Hall Polynomials, Second Edition*, Oxford Science Publication, New York (1995).
- [57] T. Royen. The distribution of the square sum of Dirichlet random variables and a table with quantiles of Greenwood’s statistic. arXiv:1008.4059 [math.ST] (2010).
- [58] T. Royen. Exact Distribution of the Sample Variance from a Gamma Parent Distribution. arXiv:0704.1415 [math.ST] (2007).
- [59] I. Weissman. Sum of squares of uniform random variables. *Statistics & Probability Letters* **129**, 147 (2017). <https://doi.org/10.1016/j.spl.2017.05.018>.
- [60] Y.-P. Förster, L. Gamberi, E. Tzanis, P. Vivo and A. Annibale. Exact and Approximate Mean First Passage Times on Trees and other Necklace Structures: a Local Equilibrium Approach. *Journal of Physics A: Mathematical and Theoretical* **55**, 115001 (2022).
- [61] A. Kells, V. Koskin, E. Rosta and A. Annibale. Correlation functions, mean first passage times, and the Kemeny constant. *Journal of Chemical Physics*. **152** (10), 104108 (2020). <https://doi.org/10.1063/1.5143504>.
- [62] L. Katz. A New Status Index Derived from Sociometric Analysis. *Psychometrika* **18** (1), 39–43 (1953).
- [63] V. Domínguez-García and M. A. Muñoz. Ranking species in mutualistic networks. *Scientific Reports* **5** (8182), 1–7 (2015).
- [64] P. Chen, H. Xie, S. Maslov and S. Redner. Finding scientific gems with Google’s PageRank algorithm. *Journal of Informetrics* **1** (1), 8–15 (2007).
- [65] J. Sherman and W. J. Morrison. Adjustment of an Inverse Matrix Corresponding to a Change in One Element of a Given Matrix. *Annals of Mathematical Statistics* **21** (1), 124–127 (1950). doi: 10.1214/aoms/1177729893.
- [66] Vincent Thibeault, Antoine Allard and Patrick Desrosiers. The low-rank hypothesis of complex systems. Preprint arXiv:2208.04848 (2022).